



MASTER'S DEGREE IN SMART GRIDS

MSc DISSERTATION

MV Grid Discovery via Phasor Measurement Units

Author: Maximiliano Pérez López

Industrial Advisor: Michele Negro

Academic Advisor: Andrés Tomás Martín

Madrid

15th of August of 2025

I declare, under my responsibility, that the Project submitted with the title

MV Grid Discovery via Phasor Measurement Units

to the ETS School of Engineering - ICAI at Universidad Pontificia Comillas

in the 2024/25 academic year is my own work, original and unpublished,

and has not been previously submitted for any other purpose.

The Project is not a total or partial plagiarism of another work,

and all information taken from other documents is properly referenced.




Signed: Maximiliano Pérez López

Date: 15/ 08/ 25

Authorized project submission

PROJECT ADVISOR



Signed: Andrés Tomás Martín

Date: 15/ 08/ 25

Acknowledgements

I would like to express my appreciation to my advisors, Andrés Tomás Martín and Michele Negro, for their support, guidance, and feedback in the development of this project.

I also want to thank the engineers at the Gridspertise laboratories, for their experience in this topic was of great support.

I am deeply grateful for the endless support and understanding my father, my mother, and my brother have given me throughout this part of my journey.

ABSTRACT

This thesis project studies PMU-based fault location in medium-voltage distribution networks with a focus on solutions that a utility could actually deploy. The core of the work aims to discover if a single-ended impedance estimator, supported by a small set of well-placed PMUs can deliver reliable locations without instrumenting the entire feeder. To keep costs realistic, PMUs are assumed at sites where previous monitors already exist. The choice is tied to quality of service, since quicker and more trustworthy location shortens isolation and restoration.

A 43-node section of an urban Milan feeder serves as the case study. Faults are simulated across nine scenario families that combine three fault types with three fault-resistance levels of 0, 1, and 5 Ω . Phasors are extracted, apparent impedances are computed, and each PMU produces a location probability over the network. These per-sensor views are then combined through a Bayesian rule under a uniform prior. Performance is reported using correct-classification rate, posterior probabilities, and distance error both in metres and as a share of feeder length. For context, a baseline using only the head-end sensor is evaluated alongside the fused method.

The method resulted in three main findings. At low resistance the method performs strongly, in several 0 Ω cases it identifies 41 of 43 events, and the associated posteriors are high. As resistance increases, confidence and hit rate decline, which accords with established accounts of one-ended impedance methods, where the additional voltage drop across the fault is read as extra line length. Even so, the 5 Ω group shows average spatial errors that remain local, roughly 3.2 percent of feeder extent, keeping switching and patrol efforts near the true section. Against the single-sensor baseline, correct classifications fall by about a quarter at 0 and 1 Ω , and distance errors rise slightly. The results suggest a credible path for DSOs: incremental PMU deployment at legacy sites, a transparent impedance estimator, and probability-based fusion.

CONTENT INDEX

Abstract *IV*

Content Index..... 5

Figures Index..... 7

Table Index 8

Chapter 1. Introduction..... 9

1.1 Alignment with the Sustainable Development Goals (SDGs)..... 10

1.1.1 Goal 7: Affordable and Clean Energy 11

1.1.2 Goal 9: Industry, Innovation and Infrastructure..... 11

1.1.3 Goal 11: Sustainable Cities and Communities..... 11

Chapter 2. State of the Art..... 12

2.1 Overview of PMUs..... 12

2.1.1 Brief History 12

2.1.2 Operation..... 13

2.2 Current Applications of PMUs in HV Transmission Networks 15

2.2.1 Common Applications..... 15

2.2.2 Fault Location Methods in Transmission Networks..... 16

2.2.3 Other Approaches..... 20

2.2.4 Summary..... 21

2.3 PMUs in MV Distribution Networks 22

2.3.1 Applications..... 22

2.3.2 Challenges of PMU Implementation in MV Networks 22

2.4 Standards and Regulations in PMU Implementation 23

Chapter 3. Project Definition 26

3.1 Justification 26

3.2 Objectives..... 28

3.3 Methodology 29

3.3.1 Gridspertise and Industrial Collaboration	29
3.3.2 Research Tools and Procedures	30
3.4 Planning and Economic Estimation	34
3.4.1 Project Planning.....	34
3.4.2 Economic Estimation.....	35
Chapter 4. Model & Algorithm Developed	37
4.1 MV Distribution Grid	37
4.2 RTDS Model	39
4.3 MATLAB System	40
4.3.1 Data Acquisition and Initial Organisation.....	41
4.3.2 Stage 1: Traditional Distance Protection	42
4.3.3 Stage 2: PMU Refinement.....	46
Chapter 5. Results and Discussion.....	49
5.1 Results	49
5.1.1 3-Phase Faults.....	50
5.1.2 Double-line-to-ground.....	60
5.1.3 Line-to-line	68
5.2 Discussion	73
5.2.1 Overall Behaviour	73
5.2.2 Comparison vs. Baseline Case.....	77
Chapter 6. Conclusions and Future Work.....	80
Chapter 7. Bibliography	84
Chapter 8. Annexes.....	92
8.1 Annex A: Source Code	92
8.1.1 Main Script	92
8.1.2 Impedance Method Function	95
8.1.3 DFT Function	99
8.1.4 Fault Classifier.....	103

FIGURES INDEX

Figure 1. History of PMU technology [3]	12
Figure 2. Diagram showing PMU operation [4].	14
Figure 3. MV Grid.	37
Figure 4. Waveform signal for the algorithm. Y axis: current (kA); X axis: time (s).	43
Figure 5. Impedance location.	44
Figure 6. Unfiltered current signal. Y axis: current (kA); Y axis: time (s)	45
Figure 7. Average Estimation Probability (%)	74
Figure 8. Number of Correct Estimations (%)	75
Figure 9. Estimation Error Distance (%)	76
Figure 10. Percentage of Correct Estimations.	77
Figure 11. Distance to Actual Fault (%).	78

TABLE INDEX

Table 1. 3-Phase $FR=0\Omega$ Fault Estimation Results.	50
Table 2. 3-Phase $FR=1\Omega$ Fault Estimation Results.	53
Table 3. 3-Phase Distance Error $FR=1\Omega$	55
Table 4. 3-Phase $FR=5\Omega$ Fault Estimation Results.	56
Table 5. 3-Phase Distance Error $FR=5\Omega$	58
Table 6. DLG $FR=0\Omega$ Fault Estimation Results.	60
Table 7. DLG $FR=1\Omega$ Fault Estimation Results.	62
Table 8. DLG $FR=5\Omega$ Fault Estimation Results.	65
Table 10. DLG Estimation Error distance.	66
Table 11. LL $FR=0\Omega$ Fault Estimation Results.	68
Table 12. LL $FR=1\Omega$ Fault Estimation Results.	70
Table 13. Error distances (km)	72

Chapter 1. INTRODUCTION

The first electric power system (EPS) was developed in 1882 by Thomas A. Edison. It was a direct current (DC) system with the purpose of supplying energy to a small portion of the area of Manhattan in New York City [1]. Over the next 143 years that followed, EPSs have become an irreplaceable aspect of modern societies. Many, if not all, of our day-to-day activities are currently powered by electricity; offices, houses, hospitals, transport, they all depend on the supply of electrical energy to keep their function. Consequently, this has placed a great responsibility on the electrical industry to deliver safe, clean, and cheap energy to the rest of the industries. This involves the crucial concept of quality of service (QOS).

Due to the elevated dependency on electrical energy, cities and countries have increased their need for a continuous energy supply, and the constant reduction of interruption times. This is part of what is considered QOS, which focuses on guaranteeing the overall quality of the energy delivered from the power systems to the final customers, as well as the energy transfer between different sections of the grid.

One of the main causes of service interruptions in electrical networks are faults. Faults have many potential origins, from weather conditions, equipment malfunction, or even human error, faults negatively affect the grid's stability. Therefore, when a fault occurs, it is crucial to locate it as quickly and as accurately as possible, as the time taken to find and isolate the affected section will determine how long customers remain with interrupted supply. This turns fault location into an essential process for protection systems in EPS.

There are several traditional fault location methods, some of them still widely used, but they will face limitations when applied to modern grids. Traditional methods' accuracy may decrease as the grid becomes more complex, and the penetration of distributed generation keeps increasing. In the past years, this has led to the development of more advanced fault location techniques that can better adapt to current power system conditions. Among these, Phasor Measurement Units (PMUs) have gained much attention.

PMUs are able to provide time-synchronised measurements of voltage and current phasors from different points in the network. This allows operators to analyse faults with a higher level of precision, as the measurements from separate locations can be compared directly. PMU technology can be used along with traditional impedance-based fault location algorithms, which could reduce the uncertainty of the estimated location and facilitate the distribution system operators (DSOs) job at reestablishing power.

However, deploying PMUs across a distribution network can be a costly modernisation. Therefore, DSOs may be interested in strategies that reduce installation and maintenance costs without losing their benefits. Here is where a new approach is needed, to install PMUs in the same positions where existing measurement devices are already present, avoiding the need for additional infrastructure.

This project follows this approach and applies it to a section of a medium-voltage distribution grid located in Milan, Italy. The method combines a more traditional impedance-based fault location with a probabilistic refinement process that merges different location predictions into a single result. This is done using Bayes' Theorem, which allows the results from different PMU perspectives to be weighted and combined according to their likelihood. The performance of this method is evaluated by simulating different types of faults and fault resistances, comparing the intended result and the actual estimation.

1.1 ALIGNMENT WITH THE SUSTAINABLE DEVELOPMENT GOALS (SDGs)

This section focuses on describing how the project relates to the United Nations' Sustainable Development Goals. The main focus is on Goals 7, 9, and 11. The connection mostly comes from an improvement in grid observability and faster fault handling when PMU-based location is applied in distribution networks. The key points are outlined below. [21]

1.1.1 GOAL 7: AFFORDABLE AND CLEAN ENERGY

The proposed PMU-based fault location supports wider and more reliable access to electricity. When faults are found more quickly and with a higher confidence, interruptions shorten and thus technical losses reduce. Both of these effects may help improve service quality and cost. In systems that include renewable generation, a grid that returns to normal operation sooner is also a grid that can host more variable resources without frequent curtailment. While the exact numbers will depend on each feeder, the direction is this: a better location helps a cleaner and more dependable supply, which aligns with Goal 7. [21]

1.1.2 GOAL 9: INDUSTRY, INNOVATION AND INFRASTRUCTURE

This work is a step in a continuous process of modernising electrical infrastructure. An important part of the proposal involves that PMUs are placed where monitors already exist, and that their measurements are combined to produce a final estimation. In this way, fault management improves without the need for full-network instrumentation, which promises to keep costs and maintenance at lower levels for DSOs. These features match Goal 9's emphasis on resilient infrastructure and innovation grounded in real operational constraints. [21]

1.1.3 GOAL 11: SUSTAINABLE CITIES AND COMMUNITIES

Urban areas depend on continuous electricity for transport, healthcare, communications, and many other daily activities. Long-lasting supply interruptions can disrupt all of these activities. Faster and more accurate location will reduce restoration times and stabilise operations during disturbances. Even small improvements at feeder level can contribute to resilience. This is in line with Goal 11's aim to reduce the impact of disruptions and to support reliable services for communities. [21]

Chapter 2. STATE OF THE ART

2.1 OVERVIEW OF PMUS

Phasor Measurement Units (PMUs) are measuring devices designed for monitoring, protection, and control within power systems. These devices have been present in electrical power systems (EPS) for the past 50 years and they have become one of the most promising options for providing efficient, accurate, and reliable measurement data for protection and monitoring schemes.

2.1.1 BRIEF HISTORY

Their development began in the early 1970s along with the Symmetrical Component Distance Relay (SCDR) [2]. Since then, the multiple algorithm proposals in the 70s and the development of the GPS satellite system made the creation of the first PMU prototype possible in 1988. However, that was merely a prototype, and it was not until 1991 that the first commercial PMU was released [3], which in the following decades continued to evolve into a more efficient, reliable technology. This technology has since become essential to the development, maintenance, and protection of smart grids worldwide.

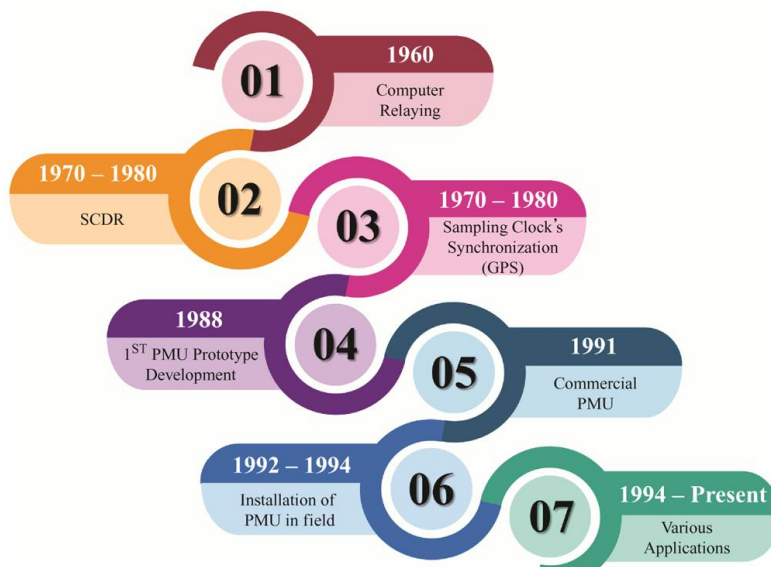


Figure 1. History of PMU technology [3]

One of the main features that makes PMUs so attractive is their use of global positioning system (GPS) signals to provide precise timing signals. GPS synchronisation enables them to provide synchronised measurements of voltage and current phasors. This means they can measure voltage and current phasors, and the frequencies of the voltage phasors with precise time synchronisation [3]. This allows them to synchronise measurements across the grid with very high accuracy [4]. This turns them into devices that are well suited for applications such as state estimation, fault detection and location, protection, and other time-sensitive related applications.

These devices play an essential role in enhancing performance, reliability, efficiency, and safety in EPS.

2.1.2 OPERATION

The structure of PMU-based protection systems can be sectioned into their hardware and their software portions.

2.1.2.1 Hardware

The physical installation of PMUs can be explained by its basic, most essential phases, presented in the following process:

- In the first stage, voltage and current magnitudes are lowered through potential and current transformers (PTs and CTs).
- Then, once the signals are at an appropriate level, they are sent through a low pass filter to prevent aliasing.
- After that comes the most important section of the measurement process. The signals are synchronised by assigning a Universal Coordinated Time (UTC) timestamp to each one. These are received in the GPS receiver that obtains the synchronisation pulses from GPS satellites.

- Once this stage is over, the now synchronised signals are digitised in the analog-to-digital converter.
- The processing unit extracts the voltage and current phasors from the received signals by using a phasor estimation algorithm.
- Finally, the synchrophasors, with their respective timestamps, are sent to the control centres by using the communication infrastructure [4].

Figure Ov1 shows a diagram of the operation previously explained.

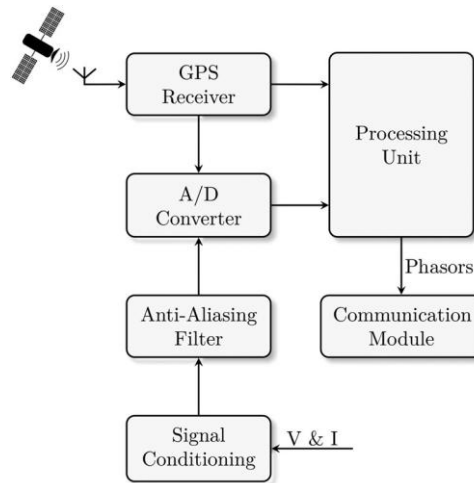


Figure 2. Diagram showing PMU operation [4].

Naturally, PMU deployment requires the installation of a communication infrastructure capable of transmitting a great amount of

2.1.2.2 Software

Regarding the software side of PMU operations, phasor estimation algorithms are the area of research with the most extensive presence in literature. There is a large volume of studies analysing and comparing existing algorithms, as well as proposing new approaches. The review [4] presents an extensive comparison of papers encompassing the last 25 years, mainly focusing on PMU phasor estimation algorithm research.

2.2 CURRENT APPLICATIONS OF PMUS IN HV TRANSMISSION NETWORKS

There is a large volume of published studies describing the role of PMUs in high voltage (HV) transmission networks. An increasing amount of literature is being published on the use of these devices for many applications such as fault detection and location, distance protection, stability, and Wide Area Monitoring System (WAMS). Recent developments in the field of power systems have led to a renewed interest in PMU-based protection schemes. The general consensus in the literature is that they improve stability, reliability, and efficiency.

2.2.1 COMMON APPLICATIONS

2.2.1.1 Monitoring and Control

PMUs can provide precise and synchronised measurements, useful for advanced control strategies, grid automation, and system optimization. Thanks to this, PMUs contribute significantly to real-time monitoring of power systems. They offer Transmission System Operators (TSOs) detailed measurements of voltage and current phasors, which are crucial for identifying disturbances and assessing the overall health of the power system [3].

2.2.1.2 System Stability and Efficiency

PMUs are vital for enhancing system stability and operational efficiency in smart grids. Their measurements help in state estimation and voltage stability assessment [3].

2.2.1.3 Fault Detection

PMU technology has become instrumental in fault detection within the power grid. The microsecond accuracy allows for precise detection of disturbances like frequency variations and voltage instabilities.

The growth in the adoption of PMUs reflects their important role in improving the monitoring and control mechanisms of power grid operations, providing the accuracy and reliability necessary for modern grid management [3].

PMUs are used for wide-area fault detection and location, employing analytical methods that utilize dispersed synchrophasor measurements and bus impedance matrices to detect fault inception. This allows for the determination of the faulted zone, diagnosis of the suspected faulted line, and identification of the exact fault point along the line.

They can also detect multiple faults across a wide area network using signal processing approaches, where PMUs installed at various buses acquire synchronised voltage phasors [4].

These applications are all extremely useful for transmission line protection schemes, as well as monitoring. However, the focus of this study is fault location, so the document will gravitate towards that.

Fault location is a crucial area of research for EPS. Data extracted using PMU device has proven to be useful for improving traditional fault location methods, as well as opening the way for new, innovative approaches.

2.2.2 FAULT LOCATION METHODS IN TRANSMISSION NETWORKS

IEEE Standard C37.114-2004 [5] mentions two different types of fault location methods. The first method, based on the estimation of line impedances, is often called in the literature as impedance-based. Impedances are commonly obtained using the equations developed and published by J.R. Carson, *et al.* in 1926 [6]. Naturally, the accuracy of this method depends on the accuracy of the impedance estimation method, which is high for Carson's equations.

A second method, often referred to as traveling wave, is defined by IEEE as "The resulting wave when the electric variation in a circuit takes the form of translation of energy along a conductor, such energy being always equally divided between current and potential forms" [6].

2.2.2.1 Impedance-based

Impedance-based methods can be divided into two main categories: one-ended, known as single-ended, and two-terminal, also referred to as double-ended. These methods are explained below.

2.2.2.1.1 Single-ended

Single-ended, or one-ended, fault location techniques are widely used in transmission and distribution systems to estimate the location of faults using electrical measurements obtained exclusively from one terminal of the line. These methods are typically embedded in microprocessor-based protective relays and require specific equipment and data inputs to operate effectively.

The fundamental idea behind single-ended fault location techniques lies in estimating the apparent impedance seen from a single measurement point into the transmission line. This estimated impedance is then used to infer the distance to the fault. In order to obtain accurate results, it is generally necessary to measure phase-to-ground voltages and the corresponding phase currents across the three phases. However, phase-to-phase faults remain detectable even if only line-to-line voltage data is available. Furthermore, if the zero-sequence source impedance is known, estimates of phase-to-ground faults can also be obtained.

One of the simplest implementations of this approach is known as the reactance method. In this case, the fault distance is assumed to be proportional to the ratio between the measured reactance and the total line reactance.

In order to properly apply these methods, there are mainly three crucial components that these systems must possess. Firstly, measurement equipment, typically a digital relay, that is capable of capturing voltage and current signals and performing the corresponding impedance-based calculations. Secondly, the system needs to be able to guarantee accurate data acquisition, for this most algorithms rely on voltage and current measurements. The algorithm must be able to identify the faulted phases. In some cases, this process is aided by including pre-fault load data to improve the overall accuracy. Finally, a communication

interface is essential to allow the remote access of the fault location estimates. This is normally carried out in many TSOs by Supervisory Control and Data Acquisition (SCADA) systems.

Unfortunately, single-ended methods are subject to various situations that can potentially impact their accuracy. For example, the presence of high levels of load current and fault resistance can significantly affect the estimation. This is evident in basic reactance methods. As these assume negligible resistance and load, they tend to be especially sensitive to these deviations. Another of these examples could be the incorrect identification of the faulted phases, which would lead to a mislead in the impedance calculation, ultimately resulting in inaccurate location estimates.

Other inaccuracies may also be introduced from the assumptions inherent in the line modelling process. For example, assuming perfect transposition or neglecting the impact of charging capacitance can result in discrepancies between actual and modelled system behaviour. In a similar way, the presence of system elements such as shunt capacitors or reactors can alter the impedance profile observed from the relay. This affects the resulting fault location estimation. It is also possible for unbalanced pre-fault load flow to distort the waveforms used by the algorithm, leading to measurement errors. These can be the result of errors present in the CTs and PTs, the analog-to-digital converter, or the filters, reducing reliability, especially for transient faults where steady-state conditions are not achieved.

To address these limitations, various algorithmic strategies have been developed over the years. The simple reactance method ignores the resistive component of the fault path, which in turn makes it less effective facing high-resistance faults and heavily loaded systems. Other, more complex techniques, such as the Takagi method and other superposition-based approaches, appear to improve accuracy by removing the load current with a differential current term. These methods intend to increase the robustness against unbalanced conditions, although they may still be sensitive to heavy variations in the system impedance.

Overall, single-ended fault location methods present the advantage of being able to provide practical solutions without losing their cost-efficient characteristics by reducing

infrastructure requirements, identifying fault locations by using data from only one terminal. While this approaches face various challenges, continuous improvements in algorithms can counter them and answer to the needs of the TSOs and DSOs using them.

2.2.2.1.2 Double-ended

Double-ended, or two-terminal, fault location methods utilize data collected from both ends of a transmission line to determine the location of the fault. These methods are generally more accurate than one-ended techniques due to their ability to mitigate common sources of error.

Unlike single-ended methods that rely solely on local measurements, double-ended methods use voltage and current data from both ends of the line. This comprehensive data allows for more accurate calculations. One of the main advantages of these methods is their ability to minimize the negative effects of variations such as fault resistance and load current in their predictions, which are one of the major sources of error in single-ended methods.

One of the main disadvantages of double-ended methods is, naturally, their need to gather data from both ends and then process it at a single location. This characteristic turns the data acquisition and processing into much more complex stages than those in single-ended methods. Another important disadvantage is their speed. These location techniques generally require more time to generate an estimate, and although speed may not be critical for some applications, a longer location estimation time can lead to longer downtime and interruptions, negatively impacting the grid's QOS.

In conclusion, double-ended methods are generally more precise in comparison to single-ended techniques. As they benefit from the data collected at both ends of the line, they can better account for fault resistance and load current. Also, they do not require prior knowledge of the fault type. Nevertheless, single-ended methods greatly benefit from their simplicity, and, consequently, their lower cost. These characteristics become especially relevant in systems where investment is limited or unavailable.

2.2.2.2 Travelling Wave

Travelling wave methods leverage the transient signals, or travelling waves, generated when a fault occurs to compute the location of the fault. These waves, travelling close to the speed of light, propagate from the fault location to the line terminals. There, the measurement devices receive the signals and timestamp them using a common time reference. [7]

These methods are also divided into the same two categories as impedance-based techniques.

2.2.3 OTHER APPROACHES

Additionally, recent advancements in fault location methods have led to the exploration of hybrid approaches that combine elements of both traditional techniques to enhance fault location accuracy. These hybrid methods take advantage of the strengths of synchronised phasor data from PMUs alongside transient signal analysis, allowing for a more complete fault detection under varying system conditions. For example, integrating impedance measurements with travelling wave analysis can significantly improve the precision of fault localisation, especially in complex distribution networks where multiple factors may influence the signal integrity [8]. Furthermore, the implementation of machine learning algorithms in conjunction with these hybrid methods has shown promise in optimising fault location processes by adapting to real-time data variations and learning from historical fault patterns [9]. This fusion of technologies has demonstrated to be a promising approach to improve EPS's detection capabilities.

In Ref. [10], the authors propose a new, interesting method that tackles the challenges of fault location. This method integrates data from a limited number of PMUs and smart meters by transforming all measurements into a unified linear form, allowing their use in a weighted least squares state estimation model. The method includes zero-injection constraints and accounts for measurement uncertainty, obtaining an accurate estimation of network states under fault conditions.

To improve efficiency, the network is divided into subregions, and the fault region is identified by analysing current imbalances derived from pre-fault and post-fault

measurements. Within the identified region, each node is tested as a hypothetical fault point by injecting a virtual fault current and recalculating the system state. The node that minimizes the weighted measurement residual is selected as the fault location. This process is extended over a short time window to improve its resilience against noise.

The approach was tested on a modified IEEE 33-node system. The results show that the method achieves high accuracy across different fault types and resistances, outperforming existing techniques while requiring fewer measurement devices and less computational effort.

Ref. [11] proposes a novel method that uses smart meter data to more accurately determine faulty points. A key advantage of this technique is its ability to use low-resolution data for identifying potential fault locations.

These new methods aim to overcome limitations of older techniques, such as those that only narrow down the fault range to the nearest nodes, which prevents precise location determination. The development of these methods focuses on improving accuracy and reliability across various fault scenarios and measurement noise levels [10].

2.2.4 SUMMARY

Although considerable research has been conducted on PMU applications in HV transmission networks, a critical gap remains in understanding their effect on MV distribution systems, especially under the increasing DER penetration. As highlighted in a review by Menezes *et al.* [4], few studies have directly examined PMU applications in real-life electrical grids. This indicates a potential limitation in the existing body of work, as most research papers focus on simulations instead of real EPS. It is important to note that this lack of experimental results may hinder the accuracy and general relevance of these data for real PMU implementation. Another problem is the lack of information regarding the methodology; this is probably due to limited access to relevant data. Consequently, further investigation targeting this gap may provide new insights into the practical implications of implementing this technology in smart distribution networks.

2.3 PMUS IN MV DISTRIBUTION NETWORKS

2.3.1 APPLICATIONS

In a review published by Menezes *et al.* [4], the authors mention different applications related to distribution systems, they particularly highlight fault detection and location, state estimation, islanding detection, and other protection schemes.

The papers reviewed are significantly fewer than those related to transmission applications. From a total of 39 research papers proposing new approaches to PMU integration in EPS, a total of 32 were focused on transmission systems, while only 8 researched distribution-level areas, with 4 of them being microgrids. However, 2 of those papers focus on general protection. That means only 1 paper from the 39 reviewed is truly relevant to fault location.

In the research paper published by Pignati *et al.* [12], it is claimed that PMU-based protection schemes possess the needed characteristics required for time-critical situations such as fault location.

2.3.2 CHALLENGES OF PMU IMPLEMENTATION IN MV NETWORKS

An important aspect to consider is the challenges that come with working in medium-voltage (MV) distribution networks. While PMUs have been extensively developed and integrated to operate in HV transmission networks, the challenges that distribution presents are not equivalent to those of transmission. This means that the particular limitations related to MV grids will have to be considered to adapt PMU technology to these new applications.

2.3.2.1 Installation and Maintenance Costs

Despite their attractive advantages, PMU deployment carries several challenges that need to be considered. One of these challenges is the costs related to installation and maintenance activities. Considering general PMU implementation costs, that is, both transmission and distribution levels.

The U.S. Department of Energy offers a brief sight of the related costs concerning these deployments in [13]. This document sheds some light on the average investment required by these devices. It shows a median of 43,400 USD per PMU installed. This value includes the cost of each device as well as every installation-related cost such as design, labour, materials, and construction.

Economies of scale do not benefit this particular type of devices. That means that there is no cost decrease associated with the large-scale PMU deployment.

Nevertheless, it is important to note that the results shown in these reports vary in magnitude (i.e. some projects presented costs double or half the median cost) [13].

However, research suggests that it is possible that through optimal PMU placement, high costs and communication infrastructure issues might be reduced. In reference [14], Cruz *et al.* propose an optimization algorithm for centralised WAMS. This paper presented an optimization algorithm that managed to reduce PMU installation costs for certain applications. This proposal was tested in various IEEE test networks, including a practical application in a 5804-bus Brazilian transmission system. The results demonstrated flexibility and effectiveness, with a promising scalability and adaptability. These results contradict the conclusions presented in the recovery Act from the U.S. government.

2.4 STANDARDS AND REGULATIONS IN PMU IMPLEMENTATION

The standards regulating PMUs integration primarily focus on ensuring that their performance, accuracy, and reliability in measuring electrical grid parameters is sufficient for the required applications. These standards define specific requirements for PMU functionality, measurement capabilities, time synchronisation, and evaluation methods.

To be compliant with IEEE C37-118-1:2011, a PMU must accurately provide three specific measurements:

- Synchrophasor measurements
- Frequency measurements
- Rate of Change of Frequency (ROCOF) measurement

These measurements are crucial for understanding the dynamic behaviour of power systems. The requirements for these measurements must be met consistently, regardless of whether the PMU is a standalone device or integrated into a multi-function unit. The standard also specifies methods for evaluating these measurements under both static and dynamic conditions [15].

Accurate time synchronisation is, naturally, a fundamental requirement for PMUs, as it ensures that measurements taken at different locations in the power system are correctly aligned in time. The IEC/IEEE 60255-118-1:2018 standard specifies stringent criteria for time synchronisation to guarantee the integrity of synchrophasor, frequency, and ROCOF measurements.

Each PMU must be capable of receiving a time reference traceable to UTC, typically delivered via a Global Navigation Satellite System (GNSS), such as GPS. The accuracy of this time input must be sufficient to maintain all measurement errors, particularly Total Vector Error (TVE), Frequency Error (FE), and ROCOF Error (RFE), within their defined limits.

A time synchronisation error of 1 microsecond translates to a synchrophasor phase error of approximately 0.022° in a 60Hz system or 0.018° in a 50Hz system. Given that a phase error of approximately 0.57° corresponds to a 1% TVE, the standard effectively permits a maximum time synchronisation error of $\pm 26\mu\text{s}$ for 60 Hz systems and $\pm 31\mu\text{s}$ for 50Hz systems. To ensure appropriate performance, the standard recommends that the time reference used by the PMU provides time, frequency, and stability with an accuracy at least ten times better than these values.

In addition to receiving accurate time, the PMU must generate a timestamp for each measurement. This timestamp must include the measurement time with a resolution of at least 1 μ s, and it must also convey information about time quality, traceability to UTC, and leap second status. Proper compensation for system-induced delays, such as filter group delays, is also mandated, ensuring that timestamps accurately reflect the true measurement time.

By enforcing these synchronisation requirements, the standard aims to ensure that synchrophasor data from distributed PMUs can be reliably used for analysis, control, and protection applications in modern power systems.

However, this standard has been, as of today, replaced by the newer standard IEC/IEEE 60255-118-1:2018 [16]. This more recent standard has updated the definitions of many measurands, as well as some of the compliance requirements.

Chapter 3. PROJECT DEFINITION

3.1 JUSTIFICATION

As modern power systems evolve to accommodate high levels of distributed energy resources (DERs), electric vehicles, and bidirectional energy flows, medium voltage (MV) distribution networks face increased complexity. Fault detection and location are now more challenging than ever, yet critical for protection schemes, focused on maintaining reliability and minimising downtime. Phasor Measurement Units (PMUs) offer an attractive solution by providing time-synchronised measurements. However, their adoption in MV networks has been hindered by high costs, complex installation requirements, and the traditionally dense deployment needed for effective coverage.

Research has shown that DER penetration has a negative impact in the stability and reliability of distribution networks. In a study done in 2022, M. S. Turiman *et al.* analysed and studied the technical impacts that distributed generation (DG) had in distribution grids. The consensus was that one of the main effects of DG integration was an increase in fault level, especially related to synchronous and asynchronous machines. Other findings were that DG integration had the potential to affect voltage regulation, cause voltage limit violation, increased network losses, and increased line loading [17].

However, DER not only have negative impacts, Ref. [18] studied the impact of Battery Energy Storage Systems (BESS) on distribution networks. In this paper, the authors found that BESS had a positive impact on the grid in which they were implemented. They appeared to improve stabilization by facilitating a fast response, as well as reducing the negative effects of disturbances and improving the power quality of the grid.

It is also important to note that while a low presence of DG in the grid is normally manageable, when that presence reaches a percentage higher than 20%, outages start to become much more likely and critical. Ref. [19] highlights how much DG impacts distribution networks.

This project addresses these shortcomings by developing and testing a PMU-based fault location method for MV networks that provides higher-quality data. The methodology is built around realistic data and conditions: it utilises real measurements provided by Gridspertise, along with a MATLAB Simulink simulation that accurately models the behaviour of MV distribution grids under fault conditions.

The method centres on single-ended, impedance-based fault location algorithms, chosen for their low infrastructure requirements and compatibility with existing utility devices. However, unlike traditional single-ended methods, the approach proposed in this project introduces enhancements aimed at maximising the value of each PMU by using a tailored measurement placement strategy and adapted fault analysis to compensate for the reduced observability.

The value of the proposition is clear, to use fewer PMUs to achieve accurate fault location. This can significantly reduce capital and installation costs. Faster and more efficient fault detection will minimise outage times and improve service reliability indicators like System Average Interruption Duration Index (SAIDI) and System Average Interruption Frequency Index (SAIFI). Deployment is more realistic and scalable, as the system can operate effectively even in partially monitored networks.

Using real PMU data from an industry partner improves the applicability of the approach, while the simulation testing allows for a flexible analysis of performance under diverse scenarios and fault types without the technical and economic complications of real grid testing.

This project aims to offer a commercially and operationally viable alternative to populate networks with PMU technology by balancing performance and practicality. It gives utilities a path to benefit from the protection and monitoring capabilities of PMUs without the financial and technical burden of making entirely new installations. The proposed method aligns with the goals of smart grid modernisation, especially in regions where investment in new infrastructure must be carefully analysed.

In conclusion, this project aims to deliver a cost-effective solution for PMU-based fault location in MV distribution systems. It combines academic content with industrial relevance, building a bridge between research and deployment. For distribution system operators (DSOs), the result is a method that provides the benefits of synchrophasor data while optimizing economic investment and reducing the need for large-scale infrastructure deployment.

3.2 OBJECTIVES

The main objective of this project is to analyse the feasibility of PMU deployment in distribution networks. This analysis consists of two main sections. First, the literature review and feasibility analysis for the implementation of PMU technology in MV grids by the company Gridspertise, and a second section focused on proposing a new algorithm approach for fault location using PMU synchrophasor data.

This second section aims to develop and evaluate a fault location method for MV distribution networks based on PMU data, with a specific focus on reducing the number of PMUs required for fault location without sacrificing their accuracy.

To achieve these goals, the project is structured around the following specific objectives:

1. Do an extensive and critical literature review of existing PMU-based fault location methods, with a particular emphasis on their applicability to MV distribution systems and their respective infrastructure requirements.
2. Identify and analyse the main limitations of current single-ended and double-ended fault location techniques, considering the context of reduced sensor deployment, DER penetration, and distribution network topology.
3. Design a fault location strategy based on single-ended impedance-based algorithms, optimising for limited PMU deployment, using real measurement data provided by Gridspertise.

4. Develop a distribution network model in MATLAB Simulink that replicates realistic MV grid conditions, to then proceed to test fault events, system behaviour, and algorithmic performance.
5. Simulate and test the proposed fault location algorithm under a range of fault scenarios, including varying fault types.
6. Compare the proposed approach against a baseline method, such as a traditional single-ended impedance-based algorithms to highlight the implications and advantages of the proposed PMU strategy.

Through these objectives, the project aims to contribute a validated, efficient, and practical approach to fault location in MV networks, supporting the adaptability of smart grids while minimising investment in hardware and communication infrastructure.

3.3 METHODOLOGY

This project follows a multi-phase methodology that integrates a systematic literature review (SLR), an algorithm development, a simulation-based validation, and a feasibility analysis. The aim of the first phase of the project is to extensively review the existing literature regarding PMU devices, fault location, and medium voltage networks. The second phase focuses on the design and evaluation of a novel fault location algorithm for MV distribution networks using synchronised phasor data obtained from PMUs. The final phase, the feasibility analysis, intends to determine whether it is viable or not for the company Gridspertise to implement PMU technology in MV smart grids.

3.3.1 GRIDSPERTISE AND INDUSTRIAL COLLABORATION

This project was conducted in collaboration with Gridspertise, an Enel Group company specialised in providing advanced smart grid solutions. Gridspertise served as the industrial partner and primary source of technical insight for this study. The company offered experience as well as the simulation model of a real MV distribution network with its

respective data, which was fundamental for conducting the experimental portion of this research.

3.3.2 RESEARCH TOOLS AND PROCEDURES

The research aims to investigate fault location methods in MV distribution networks using PMU data. By combining a literature review with the use of a simulation-based model provided by Gridspertise, the methodology integrates theoretical analysis, data collection, and experimental validation.

3.3.2.1 Literature Review and Reference Management

The state of the art presented in this project was developed by using an SLR approach. For that purpose, a search was conducted in several research databases such as IEEE Xplore, MDPI, and ScienceDirect, using terms relevant to the project, including “fault location”, “phasor measurement units”, “medium voltage”, “distribution networks”, “standard”, “impedance-based”, among many others. More than 150 papers published between 2000 and 2025 were reviewed. The selection criteria for them included their relevance to PMU-based fault location, their application in MV networks, and the journal’s quality. The selected studies were categorized based on their relevance, area of application, year of publication, and methodology, facilitating the identification of common techniques, limitations, and research challenges. This approach intends to make sure that the review provides a reliable foundation for the development of the proposed algorithm. This literature review used a qualitative approach to gather and analyse the information found in the research. The review process was supported by the reference manager software Mendeley, as well as Microsoft Excel. The mentioned databases were used to search a variety of research papers, conference proceedings, standards, books, and reports, with access granted by both Universidad Pontificia Comillas and the University of Strathclyde.

3.3.2.2 PMU Data and Simulation Model

This section outlines the methodology followed to develop and validate the impedance-based fault location algorithm using real fault data from a distribution network. This study uses existing measurements extracted with non-PMU devices, under the assumption that future PMUs will be installed at these same locations. This strategy leverages already available infrastructure, significantly reducing deployment costs and enabling more scalable fault location solutions.

The core idea of this work is to use existing fault measurements, originally collected by conventional monitoring devices such as RGDAT, and use them to test the PMU-based fault location algorithm. This works under the following assumptions:

- PMU devices will be installed by the DSOs in the same locations where previous measurement devices were already installed, replacing previously utilised equipment. This is important and will reduce costs and optimise their deployment. Studies and research made by the U.S. Department of Energy have proved that PMU deployment is a cost-intensive change. Naturally, DSOs will not only need to invest in each device, but also in the communications infrastructure, the sensors, CTs, and PTs required to extract the desired measurements. Due to this, there has been considerable research aiming to optimise PMU placement to guarantee the most cost-effective solution for their integration in the grid [13].

From an academic perspective, the ideal scenario for achieving the highest fault location accuracy involves optimising PMU placement specifically for the topology of the target distribution grid. This can be accomplished through the use of optimal PMU placement algorithms, which have been extensively studied in the literature in the past decade [20]. However, in practical settings, this approach may not be the most viable for DSOs, as building an entirely new infrastructure for each device is economically infeasible. Therefore, relying on existing infrastructure, including previously installed monitoring devices such as RGDMS, proves to be a more convenient approach.

To respond to that need, this project proposes a cost-effective alternative: installing PMUs at the same locations currently occupied by older measurement devices. By reusing this existing infrastructure, DSOs can significantly reduce installation and deployment costs, providing a more accessible option to introduce this technology into the networks.

By assuming that PMUs will be installed at the same measurement points in the future, this study avoids the need for costly new installations during the validation phase. Instead, the available data is processed and used to simulate how a PMU-based system would behave under the same conditions.

The methodology consists of three main stages:

1. Data acquisition and formatting
2. Model construction
3. Algorithm execution and validation

3.3.2.2.1 Data Collection and Formatting

The raw input for the study consists of real fault data collected from a MV distribution network. These measurements were obtained using traditional monitoring equipment and cover various fault events across the network.

The data is first transformed into .csv files, which contain voltage and current time series corresponding to each fault scenario. These files are used both to simulate the system behaviour and as direct input to the fault location algorithm. Additionally, a structured .xlsx file is created to represent the network model. This file includes the base electrical parameters of the grid such as line lengths and impedances and is used for building a reference model against which the fault data can be compared.

3.3.2.2.2 Model Construction

The model used in this study represents a 43-node MV feeder, reflecting real Italian distribution topology. This model is provided by Gridspertise. This is the base used to build the impedance comparison and distance estimation.

3.3.2.2.3 Algorithm Implementation

The impedance-based fault location algorithm is developed in MATLAB and builds upon a base version provided by Gridspertise. This algorithm is adapted and extended to fit the specific characteristics of the 43-node system and the structure of the available data.

The algorithm operates by:

1. Parsing the .csv files for each fault event.
2. Identifying and isolating the faulty portion of the data using a fault classifier, which filters out non-faulty or irrelevant measurements.
3. Computing the measured impedance at the time of the fault from the available phasor data.
4. Comparing the measured impedance to the reference impedance calculated from the model.

By comparing the impedance seen at a particular bus during a fault with the expected (normal) impedance profile of the network, the algorithm estimates the distance to the fault. The result is then mapped to the closest node or line segment.

3.3.2.2.4 Output and Validation

For each fault case, the algorithm produces several output plots and data tables, including:

- A comparison table between the measured impedance (during fault) and the modelled impedance (under normal conditions).

- A visual representation of the estimated fault distance across the feeder.
- Additional plots showing phase-by-phase impedance trajectories and classifier decisions.

These outputs are used to evaluate the algorithm's performance in locating faults across multiple real-world cases. The ability to accurately match fault impedance with the model's normal impedance allows the method to infer fault distance with minimal instrumentation, supporting the objective of reducing the number of PMUs required in the field.

3.4 PLANNING AND ECONOMIC ESTIMATION

3.4.1 PROJECT PLANNING

The project begins with a dedicated planning phase aimed at outlining the scope, objectives, methodology, and resource requirements. Several key activities are tackled during this stage. The decision of the milestones, definition of the tasks, and the setting of the timeline are some examples. While the original planning, including the objectives, milestones, and timeline, may still change later on, organising them early in the process facilitates facing these challenges in future phases. This foundational step is essential to guide the following phases to improve the project's efficiency, as well as to minimise potential problems in later phases.

3.4.1.1 Literature Review

The literature review starts early on the timeline, overlapping with the planning phase, with the intention to build a solid theoretical foundation. This step involves critically searching existing research on fault location techniques, PMU applications, and related topics for smart grid operation. The goal of this phase is to identify the gaps in research, competing methodologies, and the key theoretical frameworks that may aid the direction of the study.

The state-of-the-art review phase is carried out partially in parallel to the literature review. It focuses on analysing and discussing the most recent research and development, including both academical and industrial innovation. This seeks to enrich the study by bridging

algorithmic innovations with real-world applications. This phase plays a crucial role in defining for future sections the methodological approach that holds the project.

3.4.1.2 Algorithm Review

This step involves a deep analysis of existing algorithms related to impedance-based fault location. By reviewing their assumptions, limitations, and practical outcomes, this phase intends to set the stage for developing an improved adapted algorithm suitable for the data and context of the project.

3.4.1.3 Algorithm Proposal

The literature reviews are followed by a proposal of a new algorithm that adapts to the case study, answering to the needs of the company, Gridspertise. This involves turning theoretical knowledge obtained in earlier stages into a testable method. The proposal requires a considerable effort in choosing design choices, defining parameters, and preparing for future simulation and testing.

3.4.1.4 Algorithm Development and Testing

This is the most time-intensive stage of the project. During this period, the focus is on developing the main script that will carry out the fault location estimation. Later, the proposed algorithm will be tested using simulated PMU data to reflect real grid conditions and verify the algorithm's performance. This phase will require any issues that arise to be attended, and its logic refined where necessary.

3.4.2 ECONOMIC ESTIMATION

The proposed fault location scheme proves promising to provide a balance between the improvement of grid monitoring capabilities and the decrease in the cost of deploying new infrastructure. Much of this balance is achieved by assuming the installation of PMU units at locations that were previously equipped with RGDM devices, which minimises the capital investment associated with sensor deployment. This approach aims to reduce installation costs and therefore offer a more cost-efficient solution.

Finally, from a long-term perspective, a project like this attempts to contribute to the larger economic goals present in the energy transition process. Its cost-effective proposal may facilitate the integration of DERs, which is central to current decarbonization efforts. Therefore, this project explores a research area that may reduce operational costs in the short term, as well as benefiting future grid investments.

Chapter 4. MODEL & ALGORITHM DEVELOPED

4.1 *MV DISTRIBUTION GRID*

The case study selected for the development of this project corresponds to a 43-node MV distribution network, which forms part of a larger and more complex grid located in the city of Milan, Italy. Rather than implementing and testing the proposed methodology across the entire distribution system, which would have posed significant challenges in terms of complexity, computational requirements, and result interpretation, as well as time investment, a decision was made to focus the study on a smaller subsection of the grid.

This decision allowed for a more controlled and efficient evaluation of the algorithm's performance. The selected section includes 43 nodes, distributed across several radial branches and its respective amount of topological characteristics characteristic of typical urban MV networks. This portion of the grid is depicted in Figure 3.

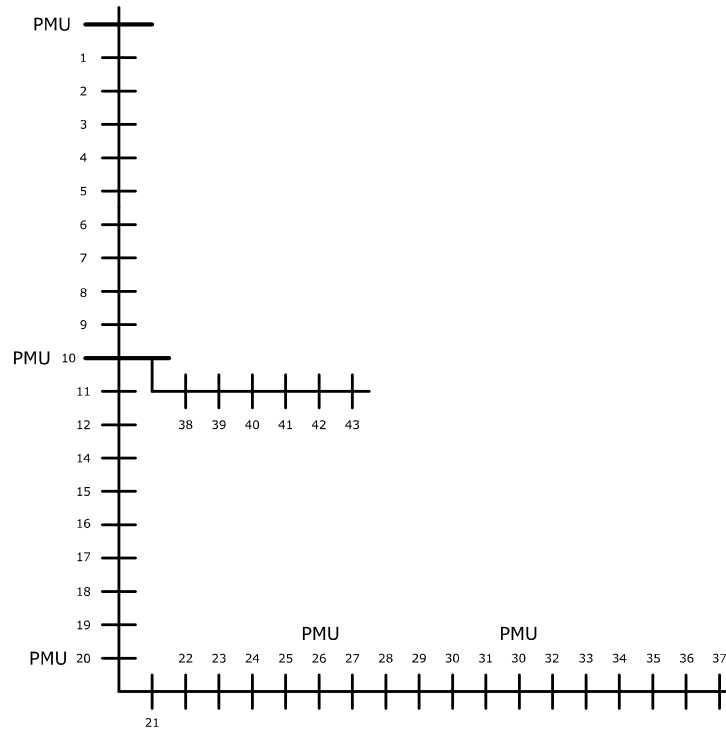


Figure 3. MV Grid.

In order to simulate the grid and apply the fault location algorithm effectively, a number of assumptions were introduced. These assumptions helped define and limit various aspects of the project, from the structure and configuration of the simulation model to the implementation and limitations of the algorithm. The most relevant assumptions are briefly described below:

- As discussed earlier, to reduce infrastructure and installation costs, PMUs are assumed to be installed in the same physical locations where previous measurement devices, which in this case study are RGDMs, were deployed. This strategy is critical to the project's cost-efficiency goal, as it uses existing infrastructure to avoid the need for significant additional investment, turning this proposal into a much more attractive option.
- Currently, due to technological limitations, it remains infeasible to obtain PMU-grade measurements directly from the header of the grid. As a result, data obtained from the header do not reflect the same level of time-synchronised accuracy as those obtained from the PMUs installed at the rest of the nodes. While this introduces a degree of uncertainty into the dataset, it represents no critical disadvantage as its impact is mitigated by the combination carried by the algorithm.
- To address the limitations introduced by the absence of a PMU at the grid header, the algorithm relies on data gathered from multiple PMUs strategically distributed throughout the network. In this specific case, five PMUs were deployed at critical locations, all of them with both remote control and RGDM sensors present beforehand. This allows the algorithm to obtain more information that then translates into a more accurate prediction method. This proposal improves the robustness of fault location predictions and compensates for any inaccuracies potentially introduced by non-PMU data sources.

The core principle behind the algorithm is the estimation of the fault distance by comparing the expected, pre-fault, line impedances with the actual impedances measured during a fault event. By doing so, the algorithm is able to calculate a set of possible distances for each

observation point. These estimated distances are then combined, and their consistency evaluated, to produce a final prediction of the fault location along with an associated likelihood or confidence level.

4.2 RTDS MODEL

To properly test the algorithm, the first step is to create a model the respective grid in a simulation software. This modelling process was conducted at the laboratories of Gridspertise in Milan, Italy, with technical support from the company. And then adapted specifically for the purposes of this study.

The model was modified to include a configurable fault component, allowing the faults to be activated at any of the 43 nodes in the network. Additionally, controllable switches were integrated to selectively activate or deactivate specific fault types. Then the resulting voltage, current, and frequency values were captured by all 5 PMU sensors and stored in folders within the software in real-time. This way, the fault location could be chosen at any point and changed whenever needed.

PMU devices were placed in their corresponding locations, header and nodes 10, 20, 26, 30. This distribution covers the entire grid and guarantees a proper observability of the grid.

The core idea was to use the model in the RTDS software to simulate in real-time the faults that were to be analysed in this study. The study focused on 9 different scenarios, which encompass 3 different fault types and 3 fault resistance values, stated as follows.

The fault types under analysis were:

- 3-Phase
- Double-line-to-ground
- Line-to-line

Similarly, these 3 fault types were simulated in 3 different fault resistance conditions, i.e., three different FR values:

- $FR = 0\Omega$
- $FR = 1\Omega$
- $FR = 5\Omega$

As each one of the three fault conditions is analysed under other three FR conditions, the results amount to nine unique simulations with individual results.

To achieve this, the model had to be simulated and automated to facilitate the extraction process. This was carried out through a script implemented in the RSCAD software that runs the RTDS simulation. This script handled the currently simulated fault location to switch from one FR value to the next, and then from one FT to the next. Each time the script finished obtaining the relevant voltage and current data, it then created a CSV file to store it and saved it in the proper folder within the device. This required the manual modification of the model to place the fault in each one of the 43 nodes within the grid.

Although the automation script streamlined much of the process, manual intervention was still required to reposition the fault component across all 43 nodes of the network, one by one. Once data had been generated for all nodes and fault scenarios, the resulting data folders were transferred to the computing environment where the main fault location (FL) algorithm was executed and evaluated.

4.3 MATLAB SYSTEM

This chapter describes the two-stage system for the automated detection and precise localisation of faults within a power distribution network. The approach integrates traditional impedance-based fault analysis with a multi-PMU data fusion technique, aiming to enhance the accuracy and reliability of fault location. The system is implemented in MATLAB, utilising a central orchestration script that interacts with many specialised functional modules, including its main: a DFT module for waveform processing, an impedance

calculation for impedance-based localisation, and a fault classifier that classifies the fault into one of 4 possible types.

The proposed system addresses the challenge of rapidly and accurately identifying fault locations by processing large volumes of simulated fault data from a Real-Time Digital Simulator (RTDS). The methodology is structured to first identify potential fault zones using individual PMU measurements (Stage 1) and then refine this localisation by probabilistically combining information from multiple PMUs (Stage 2). The main script manages the overall workflow, from data ingestion and organisation to the execution of the two analytical stages and the presentation of final fault location predictions.

4.3.1 DATA ACQUISITION AND INITIAL ORGANISATION

The initial phase focuses on efficiently loading and structuring the simulated fault data:

4.3.1.1 System Initialisation

The algorithm script starts by loading fundamental system parameters, including High Voltage (HV) network data and the detailed topology of the distribution feeder from an Excel spreadsheet. This establishes the electrical model crucial for subsequent impedance calculations.

4.3.1.2 Automated Data Ingestion

To facilitate batch processing, the user designates a single directory containing all RTDS waveform data files. These files are required to be in a Comma Separated Values (CSV) format.

4.3.1.3 Filename Scenario Grouping

A very important aspect of this stage is the appropriate organisation of the input data. Each CSV filename is created to adhere to a customised convention, N[node number]_PMU[PMU number]_[Fault type]_Rf[Fault resistance].csv. One example of this convention would be file N10_PMU1_3P_Rf_0.csv.

Where:

- N10 is the code indicating that the data in this file corresponds to a fault happening in node 10.
- PMU1 indicates that the fault data is collected by PMU 1.
- 3P represents the fault type, in this case a three-phase fault. Other fault types are represented as DLG (double line to ground) and LL (line to line).
- Rf_0 corresponds to the fault resistance, in this case 0.

This structured naming convention allows the script to automatically extract the associated PMU identifier, and the specific fault scenario (true fault node, type, and resistance), turning them into unique keys that are used later on. A programmatic structure, such as a `containers.Map`, is then utilized to group all PMU data files that correspond to the same unique fault scenario. This ensures that for a single fault event, all contributing PMU measurements are collectively accessible for analysis.

4.3.2 STAGE 1: TRADITIONAL DISTANCE PROTECTION

The first stage of the localization process makes use of conventional impedance-based principles to determine individual fault locations from the perspective of each individual PMU.

4.3.2.1 Waveform Phasor Extraction

For each PMU measurement associated with a given fault scenario, the script calls the `DFT_v7.m` model to apply the Discrete Fourier Transform to the respective waveform obtained from the CSV data. This takes the path to the raw waveform CSV file and the nominal system voltage (V_n) as inputs. Figure 4 shows the waveform signal in MATLAB.

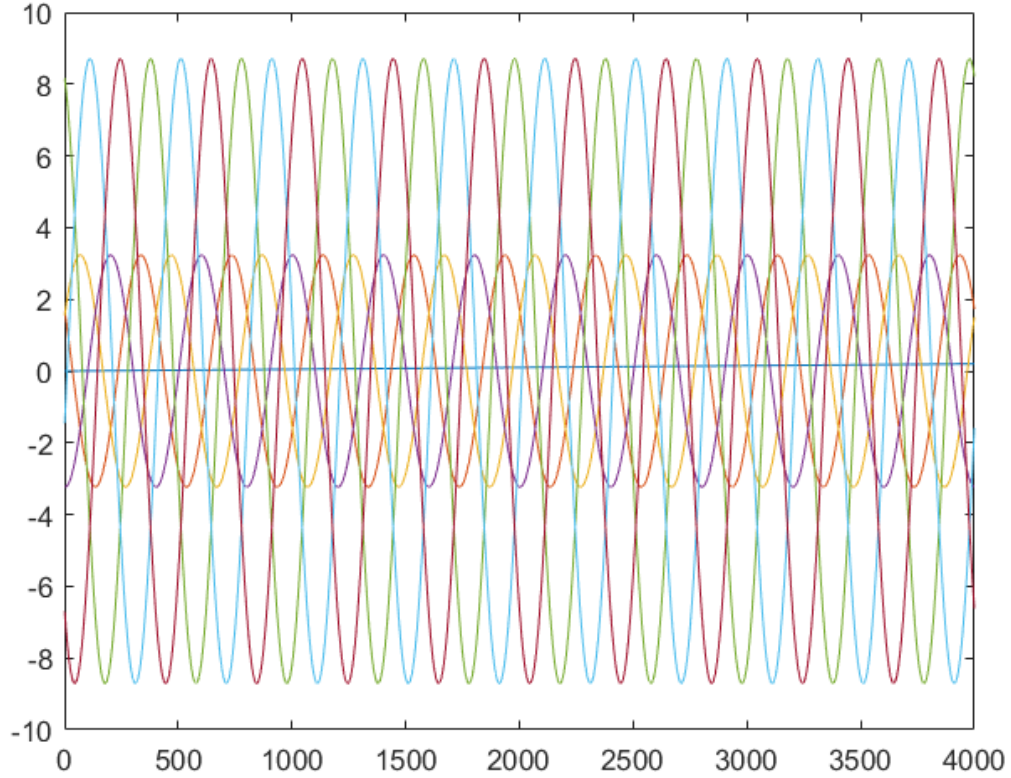


Figure 4. Waveform signal for the algorithm. Y axis: current (kA); X axis: time (s).

Within this module, the time-series voltage and current data are processed using the DFT. This function extracts the steady-state phasor components, including positive, negative, and zero sequence voltages (E_1 , E_2 , E_3 , E_{0a} , E_{da} , E_{ia}) and currents (I_1 , I_2 , I_3 , I_{0a} , I_{da} , I_{ia}). These phasor values serve as the fundamental electrical measurements for the fault analysis done in the rest of the process.

4.3.2.2 Impedance-Based Fault Zone Identification

This module receives the grid node ID corresponding to the measuring PMU, the pre-loaded grid and node topology data, HV system parameters, feeder details, nominal voltage, and the specific PMU's waveform file path.

Initially, the grid's impedance matrices (positive and zero sequence, Z_d , Z_0) are computed using the `get_imped_matrix_v5` function, establishing the electrical characteristics of each line and node. This function calculates the baseline impedances as seen from each one of the buses in the grid. This is a critical step, as the distance calculation depends on the comparison of baseline impedances and apparent impedances. In Figure 5, the results of this identification are visible.

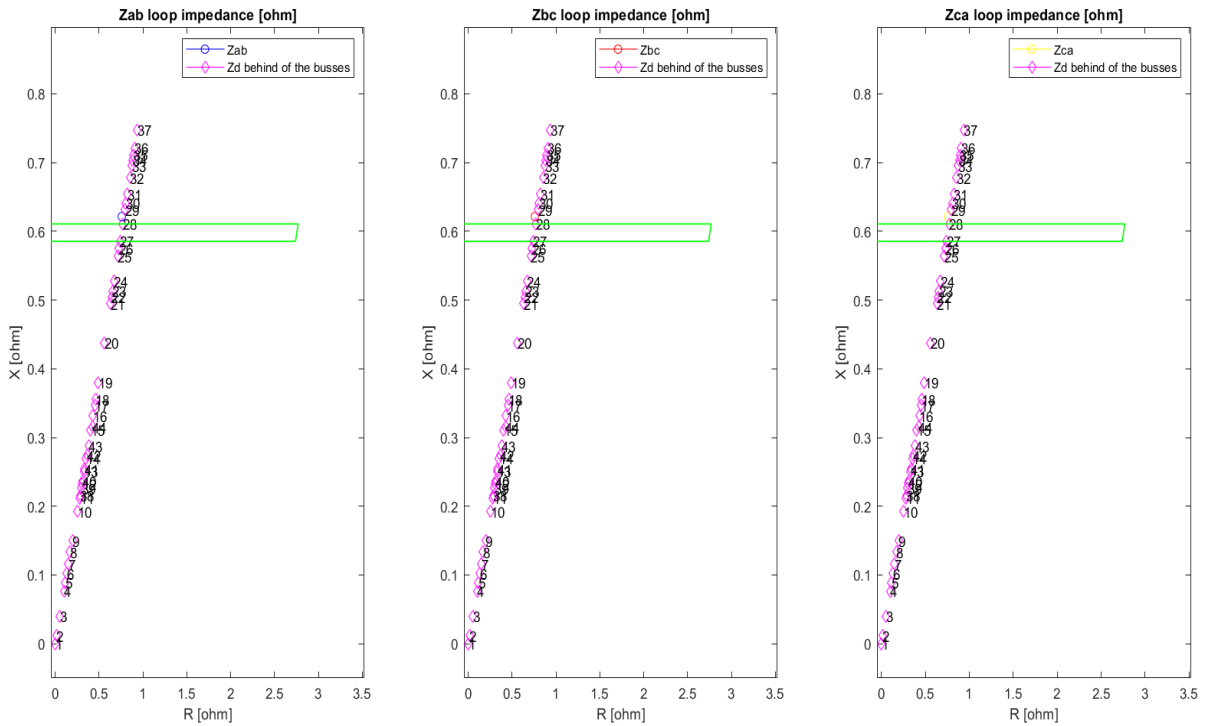


Figure 5. Impedance location.

However, the analysis results must consider the different fault types that the data might correspond to. With this in mind, a fault classifier sub-function is implemented to analyse the symmetrical components of the phasors during the fault period to determine the specific fault type (e.g., three-phase, line-to-line, or double line-to-ground). Once the fault type is calculated, there is another critical action that the script must tackle to ensure that the results are accurate.

4.3.2.3 Fault Type Filter

The script uses fault currents and voltages to calculate the apparent impedance and then makes a comparison between that and the baseline bus impedance. This information is then used to make a prediction of the fault location. However, PMUs do not always see a fault, as it may be located outside of their point of view. This may lead to false predictions as the algorithm must give a prediction regardless of the data. It is for this reason that a filter is implemented. Figure 6 shows a typical unfiltered current signal that is part of the signal inputs to the algorithm.

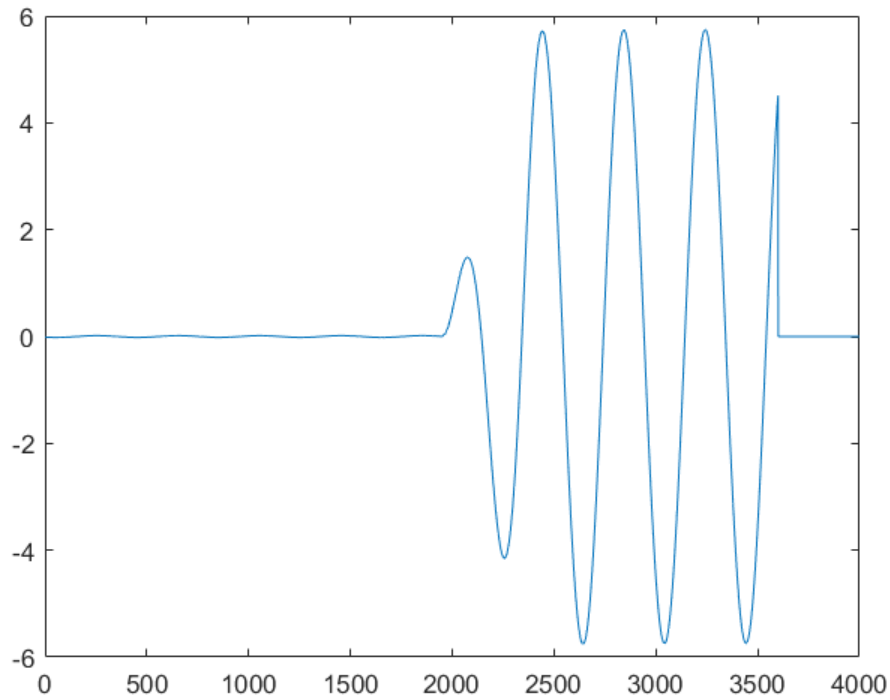


Figure 6. Unfiltered current signal. Y axis: current (kA); X axis: time (s)

Based on the fault type detected by the fault type classifier, the filter sets a series of conditions that, if met by the fault data, will classify the prediction as a “no fault” prediction. This is done by analysing the current values and based on the fault type, setting a threshold that divides fault current levels from normal current levels. This means that the data sets detected with normal current levels will have their predictions set as “no fault seen”, which provides useful information for the final prediction. The result is that if a PMU detects no

fault, then the rest of the predictions have a higher value, as the fault is not present in this zone.

4.3.2.4 Results

After the data has been filtered, the apparent impedance observed at the PMU location is calculated. This apparent impedance is subsequently mapped onto predefined MHO relay characteristic zones associated with each node in the distribution network, utilizing the Z_map function. This mapping process quantifies the likelihood that the observed fault impedance falls within the protective zone of each node.

The primary output of this stage, for each individual PMU, is a percentage vector. This vector represents a probability distribution, indicating the percentage likelihood of the fault being located at each specific node in the system, purely based on the measurements from that single PMU. For numerical stability in the subsequent stage, a small smoothing factor (ϵ) is applied to these percentages, ensuring no zero probabilities, and the vector is normalized to sum to unity.

4.3.3 STAGE 2: PMU REFINEMENT

The second stage focuses on refining the predicted fault location results by combining the individual probabilities (likelihoods) obtained from multiple PMUs using Bayes' Theorem. This integration takes advantage of several PMU measurements to improve the prediction accuracy and reduce the ambiguity inherent in the individual measurements.

4.3.3.1 Bayesian Combination of Fault Location Probabilities

The proposed algorithm relies on PMU data to estimate the location of faults in a distribution network. Due to the nature of electrical faults and the distribution of PMUs across the system, each measurement point provides a partial and independent perspective of the event. These perspectives are expressed as probabilistic fault location estimates for each possible bus in the network. In order to reach a final, consolidated prediction of the faulted location, the algorithm uses a Bayesian combination method to integrate the multiple estimates into a single, coherent probability distribution.

The core idea is to treat the outputs from different PMU viewpoints as conditionally independent likelihoods of the fault being at each node. By assuming a uniform prior probability (i.e. there is no prior knowledge for any specific node over another), the code applies Bayes' Theorem to update this prior probability using the available likelihoods.

Each iteration of the loop in the code corresponds to one group of six likelihood values (e.g., from six different PMU measurements) and for each of the 43 possible fault locations. The key steps of the algorithm are the following:

4.3.3.2 Prior Definition

A uniform prior probability distribution is assumed for all possible fault locations. Reflecting the temporary assumption that all nodes are equally likely to experience a fault.

4.3.3.3 Likelihood Aggregation

For each set of six probability columns, representing different views or methods of estimating the fault likelihood, the algorithm computes the product of the likelihoods for each location. This step combines the individual observations into a single combined likelihood for each node. This aligns with the assumption of conditional independence.

4.3.3.4 Posterior Calculation

Then, the unnormalized posterior values are computed by performing an element-wise multiplication of the prior and the combined likelihoods. This results in an intermediate vector that represents the relative belief that each node is the faulty node, before normalisation.

4.3.3.5 Normalization

To make sure that the final values represent a valid probability distribution (i.e. they sum to 100%), the unnormalized posterior is scaled accordingly. This results in the final Bayesian posterior probabilities, which are stored in a vector.

The algorithm aims to improve the robustness and reliability of the fault location prediction by combining all the different estimates through this probabilistic framework. Bayes'

Theorem allows for the fusion of independent evidence, improving its accuracy, especially in cases where some measurements may be noisy, ambiguous, or do not provide enough information when interpreted in isolation. This happens especially often when the PMU is located before a branch separation that leads to 2 or more branches with one of them containing the fault. In these cases, the PMU calculates a distance that corresponds to several different nodes, which leads to multiple predictions with similar likelihoods.

4.3.3.6 Conclusion

This two-stage methodology offers a systematic and automated approach to fault location in distribution systems. By first employing traditional impedance-based methods on individual PMU data and then efficiently combining these results using BT, the system enhances the reliability and precision of the fault location method.

Chapter 5. RESULTS AND DISCUSSION

5.1 RESULTS

As mentioned in the previous chapter, the algorithm begins the process by extracting the fault data from the CSV file that contains the measurements recorded during the fault event. Then, this information is presented in the form of waveforms to facilitate their processing. This waveform is also plotted in an effort to facilitate the visualisation of the fault behaviour, which in turn aids troubleshooting as well. The rest of the algorithm will use the voltage and current phasors in their rectangular form, $a + ib$. These values are the core of the calculations and are used throughout the entire process to calculate the impedances that will bring the results.

After reading and adapting the data, the impedance estimation stage will produce several outputs. These include the following.

- Location estimates provided by each PMU individually
- The likelihood distribution for each of the estimates
- A graph visually showcasing the comparison between the measured impedance (during the fault event) and the baseline bus values
- The voltage and current waveforms associated with the fault.

In this case study, the system includes five PMUs and one non-PMU sensor located at the header of the grid. Together, they provide a total of six separate fault location estimates. Then, in order to obtain a single final prediction, these individual estimates are combined using Bayes' Theorem. This combination step produces two outputs.

- A Bayesian combined estimate
- Probability values for each possible fault location.

It is important to note that some of the individual estimates may be, and surely will be, incorrect. This results in estimations that differ from the actual faulty node. To consider this

and allow for analysis, the distance between the estimated and the actual faulty node is calculated by computing the difference between the predicted location and the true location once the algorithm shows its results. This metric helps build a more detailed assessment of the accuracy and reliability of the proposed method.

The algorithm was tested across nine different scenarios, using three different fault resistance conditions and three unique fault types. The following sections will give a more detailed description of each of their results.

The testing worked by cycling through all the possible node faults (i.e. a file was created for each possible fault location, and the algorithm attempted to estimate correctly) and placing each final result in a table. This gives a total of 9 different tables each containing the results of 43 algorithm estimations, which also contain the combined data from 6 different sensors. This means that the analysis covers 2322 individual results, combined and categorised to facilitate their visualisation.

5.1.1 3-PHASE FAULTS

5.1.1.1 $FR = 0\Omega$

The first scenario that was analysed was a 3-phase fault with a fault resistance value of 0Ω . The estimation algorithm cycled through each one of the fault data files, assigning an estimation and its respective probability. These results are shown in Table 1, where the *Faulty Node* column indicates the real fault location, the *Final Estimated Node* indicates the algorithm estimate, and the *Estimation Likelihood* shows the probability of the estimate being correct.

Table 1. 3-Phase $FR=0\Omega$ Fault Estimation Results.

<i>Faulty Node</i>	<i>Final Estimated Node</i>	<i>Estimation Likelihood (%)</i>
2	2	99.95700698
3	3	99.95700698

4	4	99.95700698
5	5	99.95700698
6	6	99.95700698
7	7	99.95700698
8	8	99.95700698
9	9	99.95700698
10	10	99.95700698
11	11	99.99799909
12	12	99.99899932
13	13	99.99899932
14	14	99.99899932
15	15	99.99999957
16	16	99.99999957
17	17	99.99999957
18	18	99.99999957
19	19	99.99999957
20	20	99.99999957
21	21	100
22	22	100
23	23	100
24	24	100
25	25	100
26	26	100
27	27	100
28	28	100
29	29	99.99999999
30	30	100
31	31	100
32	32	100
33	33	99.99899974

34	34	99.99899974
35	35	100
36	36	100
37	1	2.272727273
38	38	99.99899932
39	39	99.99899932
40	40	99.99899932
41	41	99.99899932
42	42	99.99899932
43	43	99.99899932
44	15	99.95700698

The results shown in the table above show both the real and the estimated faulty nodes. A look at them makes it clear that the vast majority of the estimations turned out to be correct, as 41 of the 43 predictions are accurate. Regarding the estimation likelihoods, once again, the vast majority of them are above a 99.5%.

However, there are two estimations that failed to predict the correct node. When a fault happened in node 37, the algorithm did not detect any faults in the grid. When the 3-phase fault was located in node 44, the method mistakenly predicted a fault in node 15.

Taking all results into consideration, this scenario produced the following results.

- The method presents an average estimation probability of 95.34%.
- A total of 95.35% of the estimations were correct.

These results

5.1.1.2 $FR = 1\Omega$

The next case that was examined changed the fault resistance from 0Ω to 1Ω and once again, the estimation algorithm processes each of the fault data files and produces an estimated

location along with its probability. These outcomes are presented in Table 2, with the same format as previously.

Table 2. 3-Phase $FR=1\Omega$ Fault Estimation Results.

<i>Faulty Node</i>	<i>Final Node</i>	<i>Estimated Estimation Likelihood (%)</i>
2	2	99.95700698
3	3	99.95700698
4	4	99.95700698
5	5	99.95700698
6	6	99.95700698
7	7	99.95700698
8	8	99.95700698
9	9	99.95700698
10	10	99.95700698
11	11	99.99899932
12	12	99.99899932
13	13	99.99899932
14	14	99.99899932
15	15	99.99999957
16	16	99.99999957
17	17	49.98949939
18	18	99.99999957
19	19	99.99999957
20	20	99.99999957
21	22	99.99899932
22	23	99.99899932
23	23	100
24	24	100
25	26	99.99899932
26	27	99.99899932

27	27	100
28	28	100
29	29	49.99999989
30	30	49.99999989
31	31	100
32	32	100
33	33	49.99974983
34	35	99.99999998
35	36	99.99899974
36	36	100
37	1	2.272727273
38	38	99.99899932
39	39	99.99899932
40	40	99.99899932
41	41	99.99899932
42	42	99.99899932
43	43	99.99899932
44	15	99.95700698

The results in the table above display both the actual and the estimated faulted nodes. Similar to last case, these entries suggest that the great majority of estimates were correct, with, again, 41 of the 43 predictions being accurate. Regarding the estimation likelihoods, most values too exceed 99.95%.

In this case, there is a total of 8 incorrect estimations. However, the errors in this instance are of a different nature than those of the past scenario. Table 3 shows incorrect predictions on fault nodes 21, 22, 25, 26, 34, and 35. In all those cases, the estimated location was only one node away from the faulty node. This means that, while the average estimation likelihood is 76.73%, the errors in prediction are relatively small when compared to the past errors.

When computed, the distance between the faulty node and the estimated node is shown in Table 3.

Table 3. 3-Phase Distance Error $FR=1\Omega$

<i>Faulty Node</i>	<i>Final Estimated Node</i>	<i>Distance to fault (km)</i>
21	22	0.537
22	23	0.09
25	26	0.347
26	27	0.102
34	35	0.081
35	36	0.065

This yields a mean distance of 85.70m between the estimated fault and the actual fault across the entire network. When contrasted with the grid's geographical extent, this figure amounts to 1.04%. In other words, the method produces estimates with an average error of 1.04% of the analysed network.

Still, the fault in node 37 is not detected by the algorithm, and fault node 44 is still mistakenly predicted at node 15.

To summarize, this scenario produced the following results.

- The method presents an average estimation probability of 76.73%.
- A total of 81.40% of the estimations were correct.

5.1.1.3 $FR = 5\Omega$

The last 3-phase case now uses a fault resistance of 5Ω . The table structure is the same and can be seen in Table 4.

Table 4. 3-Phase $FR=5\Omega$ Fault Estimation Results.

<i>Faulty Node</i>	<i>Final Node</i>	<i>Estimated Estimation Likelihood (%)</i>
2	2	99.95700698
3	3	99.95700698
4	5	99.95700698
5	6	99.95700698
6	7	99.95700698
7	8	99.95700698
8	9	99.95700698
9	9	99.95700698
10	11	49.98949939
11	12	99.99899932
12	13	99.99899932
13	14	99.99899932
14	14	99.99899932
15	16	99.99999957
16	18	99.99999957
17	18	99.99999957
18	19	99.99999957
19	19	99.99999957
20	20	99.99999957
21	23	100
22	24	100
23	24	100
24	24	100
25	27	100
26	27	100

27	28	100
28	29	49.99999989
29	31	100
30	31	100
31	32	100
32	34	100
33	36	100
34	36	100
35	36	100
36	1	2.272727273
37	1	2.272727273
38	40	99.99899932
39	40	99.99899932
40	41	99.99899932
41	42	99.99899932
42	43	99.99899932
43	15	49.98949939
44	16	99.95700698

The results in the table above display both the actual and the estimated faulted nodes; an inspection of these entries suggests that the great majority of estimates were correct, with 41 of the 43 predictions being accurate. Regarding the estimation likelihoods, once again, most values exceed 99.95%.

Now in this scenario, most of the estimations are incorrect. The errors this time are similar to the past scenario's results. Table 5 shows all the incorrect predictions given by the algorithm. Again, most estimated locations were only one node away from the faulty node, but this time some distance errors were greater than in other cases. This results in an average estimation likelihood is 16.28%, although the errors in prediction are not as big as expected.

Table 5. 3-Phase Distance Error $FR=5\Omega$

<i>Faulty Node</i>	<i>Final Node</i>	<i>Estimated Distance to fault (km)</i>
4	5	0.335
5	6	0.118
6	7	0.127
7	8	0.127
8	9	0.168
10	11	0.390
11	12	0.174
12	13	0.189
13	14	0.170
15	16	0.381
16	18	0.334
17	18	0.146
18	19	0.080
21	23	0.627

22	24	0.174
23	24	0.084
25	27	0.449
26	27	0.102
27	28	0.102
28	29	0.240
29	31	0.294
30	31	0.094
31	32	0.125
32	34	0.223
33	36	0.311
34	36	0.146
35	36	0.065
38	40	0.309
39	40	0.100
40	41	0.100
41	42	0.151
42	43	0.176
43	15	1.951

44	16	2.379
----	----	-------

5.1.2 DOUBLE-LINE-TO-GROUND

5.1.2.1 $FR = 0\Omega$

The first DLG case considers a fault resistance of 0Ω . The table layout remains the same and appears in Table 6.

Table 6. DLG $FR=0\Omega$ Fault Estimation Results.

<i>Faulty Node</i>	<i>Final Node</i>	<i>Estimated Estimation Likelihood (%)</i>
2	2	99.95700698
3	3	99.95700698
4	4	99.95700698
5	5	99.95700698
6	6	99.95700698
7	7	99.95700698
8	8	99.95700698
9	9	99.95700698
10	10	99.95700698
11	11	99.99799909
12	12	99.99899932
13	13	99.99899932
14	14	99.99899932
15	15	99.99999957
16	16	99.99999957
17	17	99.99999957
18	18	99.99999957
19	19	99.99999957

20	20	99.99999957
21	21	100
22	22	100
23	23	100
24	24	100
25	25	100
26	26	100
27	27	100
28	28	100
29	29	99.99999999
30	30	100
31	31	100
32	32	100
33	33	99.99899974
34	34	99.99899974
35	35	100
36	36	100
37	1	0
38	38	99.99899932
39	39	99.99899932
40	40	99.99899932
41	41	99.99899932
42	42	99.99899932
43	43	99.99899932
44	15	0

The table above reports both the true and the inferred faulted nodes; reviewing these records indicates that the large majority of estimates were correct, with 41 out of 43 predictions accurate. Regarding the estimation likelihoods, again, most figures are above 99.95%. There are, however, two estimates that did not match the correct node. The case for node 37 was

the same as in 3-phase scenarios, and the algorithm did not detect the fault in the grid. On the other hand, when the three-phase fault was at node 44, the method incorrectly pointed to node 15. Taking all outcomes into account, this scenario produced the following results.

- The method presents an average estimation probability of 95.34%.
- A total of 95.35% of the estimations were correct.

5.1.2.2 $FR = 1\Omega$

The second DLG case uses a fault resistance of 1Ω . The same table format is retained and is shown in Table 7.

Table 7. DLG $FR=1\Omega$ Fault Estimation Results.

<i>Faulty Node</i>	<i>Final Node</i>	<i>Estimated Estimation Likelihood (%)</i>
2	2	99.95700698
3	3	99.95700698
4	4	99.95700698
5	5	99.95700698
6	6	99.95700698
7	7	99.95700698
8	8	99.95700698
9	9	99.95700698
10	10	99.95700698
11	11	99.99899932
12	12	99.99899932
13	13	99.99899932
14	14	99.99899932
15	15	99.99999957
16	16	99.99999957
17	18	99.99999957
18	18	99.99999957

19	19	99.99999957
20	20	99.99999957
21	22	99.99899932
22	23	100
23	23	99.99899932
24	24	100
25	26	99.99899932
26	27	99.99899932
27	27	100
28	28	100
29	30	99.99999999
30	30	49.99999989
31	31	100
32	32	100
33	34	99.99899974
34	35	100
35	36	100
36	36	100
37	1	2.272727273
38	11	33.32877718
39	12	33.32877718
40	40	99.99899932
41	41	99.99899932
42	42	99.99899932
43	43	99.99899932
44	15	99.95700698

In the table above, both the actual and the estimated faulted nodes are listed. A quick review suggests that most estimates were correct, with 33 of 43 predictions classified as accurate. As for the estimation likelihoods, most values once again exceed 99.95%. Two estimates

failed to identify the correct node. With a fault at node 37, the algorithm reported no faults in the network. With the 3-phase fault at node 44, the method wrongly predicted node 15. Considering the full set of outputs, this scenario yields the following.

- The method achieves an average estimation probability of 70.92%.
- In total, 74.42% of the estimates were correct.

For this scenario, most estimates are now incorrect. The error patterns resemble those observed previously. Table 7 summarises all wrong predictions produced by the algorithm. Once more, many predicted locations were only one node away from the true faulted node, though some distance errors are higher than in other cases. The resulting average estimation likelihood is 16.28%, even if the magnitude of the errors is lower than expected. The computed distance between the faulted node and the estimated node appears in Table 7. Overall, this leads to an average distance of 10.33m from the estimated fault to the real fault across the grid. When set against the grid's geographical span, this corresponds to 1.25%, meaning the method's average error is 1.25% of the analysed grid.

5.1.2.3 $FR = 5\Omega$

In the final three-phase scenario, the fault resistance is set to 5 Ω . The same table structure applies and is presented in Table 8.

The table below includes both the real and the predicted faulted nodes. On inspection, the vast majority of estimates are correct, with 41 out of 43 predictions accurate. With respect to estimation likelihoods, most values once again surpass 99.95%. There are two exceptions. When the fault occurred at node 37, the algorithm failed to flag any fault. When the three-phase fault was placed at node 44, the method selected node 15 instead. Aggregating the results, this scenario reports the following.

- The average estimation probability is 17.07%.
- Correct estimations account for 18.60% of the total.

Table 8. DLG FR=5Ω Fault Estimation Results.

<i>Faulty Node</i>	<i>Final Node</i>	<i>Estimated Estimation Likelihood (%)</i>
2	2	99.95700698
3	3	99.95700698
4	5	99.95700698
5	6	99.95700698
6	7	99.95700698
7	8	99.95700698
8	9	99.95700698
9	9	99.95700698
10	11	49.98949939
11	12	99.99899932
12	13	99.99899932
13	14	99.99899932
14	14	99.99899932
15	16	99.99999957
16	18	99.99999957
17	18	99.99999957
18	19	99.99999957
19	19	99.99999957
20	20	99.99999957
21	23	100
22	24	100
23	24	100
24	24	100
25	27	100
26	27	100
27	28	100
28	29	49.99999989

29	31	100
30	31	100
31	32	100
32	34	100
33	36	100
34	36	100
35	36	100
36	1	2.272727273
37	1	2.272727273
38	40	99.99899932
39	40	99.99899932
40	41	99.99899932
41	42	99.99899932
42	43	99.99899932
43	15	49.98949939
44	16	99.95700698

At this point, most estimations in this scenario are incorrect. The error types are comparable to those seen earlier. Table 10 lists every incorrect prediction generated by the algorithm. Many estimates land just one node away from the faulted node, although a few distance errors are larger than in other cases. This produces an average estimation likelihood of 17.07%, even though the overall error magnitudes are not as high as anticipated. The distance between the true faulted node and the estimated node is reported in Table 10. Across the grid, the mean distance between the predicted and actual fault positions is 270.9m. Relative to the grid's geographic extent, this equals 3.27%. In short, the method yields an average error of 3.27% of the analysed grid.

Table 9. DLG Estimation Error distance.

<i>Faulty Node</i>	<i>Final Node</i>	<i>Estimated Distance to Fault (km)</i>
4	5	0.335
5	6	0.118
6	7	0.127
7	8	0.127
8	9	0.168
10	11	0.39
11	12	0.174
12	13	0.189
13	14	0.17
15	16	0.381
16	18	0.334
17	18	0.146
18	19	0.08
21	23	0.627
22	24	0.174
23	24	0.084
25	27	0.449
26	27	0.102
27	28	0.102
28	29	0.24
29	31	0.29418
30	31	0.09418
31	32	0.12483
32	34	0.388
33	36	0.311
34	36	0.146
35	36	0.065

38	40	0.309
39	40	0.1
40	41	0.1
41	42	0.151
42	43	0.176
43	15	1.951
44	16	2.379

5.1.3 LINE-TO-LINE

5.1.3.1 $FR = 0\Omega$

This last 3-phase test adopts a fault resistance of 0Ω . The identical tabular layout applies and can be found in Table 11.

Table 10. LL $FR=0\Omega$ Fault Estimation Results.

<i>Faulty Node</i>	<i>Final Node</i>	<i>Estimated Estimation Likelihood (%)</i>
2	2	99.95700698
3	3	99.95700698
4	4	99.95700698
5	5	99.95700698
6	6	99.95700698
7	7	99.95700698
8	8	99.95700698
9	9	99.95700698
10	10	99.95700698
11	11	99.99799909
12	12	99.99899932
13	13	99.99899932
14	14	99.99899932

15	15	99.99999957
16	16	99.99999957
17	17	99.99999957
18	18	99.99999957
19	19	99.99999957
20	20	99.99999957
21	21	100
22	22	100
23	23	100
24	24	100
25	25	100
26	26	100
27	27	100
28	28	100
29	29	99.99999999
30	30	100
31	31	100
32	32	100
33	33	99.99899974
34	34	99.99899974
35	35	100
36	36	100
37	1	2.272727273
38	38	99.99899932
39	39	99.99899932
40	40	99.99899932
41	41	99.99899932
42	42	99.99899932
43	43	99.99899932
44	15	99.95700698

As shown above, the table lists both the true faulted node and the algorithm's estimate. A closer look indicates that the majority of estimates were right, with 41 of 43 predictions accurate. For the estimation likelihoods, most entries are again above 99.5%. Two estimates did not match the ground truth. With a fault at node 37, the algorithm detected no fault in the grid. With the 3-phase fault placed at node 44, the method incorrectly chose node 15. Summing up, this scenario leads to the following.

- The average estimation probability stands at 95.34%.
- In total, 95.35% of the predictions were correct.

This results in an average separation of 5.66m between the estimated and actual fault locations across the grid. Compared to the grid's geographic reach, this is 0.68%, meaning the method's average error amounts to 0.68% of the analysed grid.

5.1.3.2 $FR = 1\Omega$

In this second LL scenario, the fault resistance is set to 1Ω . The same table structure applies and is presented in Table 12.

Table 11. LL $FR=1\Omega$ Fault Estimation Results.

<i>Faulty Node</i>	<i>Final Node</i>	<i>Estimated Estimation Likelihood (%)</i>
2	2	99.95700698
3	3	99.95700698
4	4	99.95700698
5	5	99.95700698
6	6	99.95700698
7	7	99.95700698
8	8	99.95700698
9	9	99.95700698
10	10	99.95700698
11	11	99.99899932

12	12	99.99899932
13	13	99.99899932
14	14	99.99899932
15	15	99.99999957
16	16	99.99999957
17	18	0
18	18	99.99999957
19	19	99.99999957
20	20	99.99999957
21	22	0
22	23	0
23	23	99.99899932
24	24	100
25	26	0
26	27	0
27	27	100
28	28	100
29	30	0
30	30	49.99999989
31	31	100
32	32	100
33	34	0
34	35	0
35	36	0
36	36	100
37	1	0
38	11	0
39	12	0
40	40	99.99899932
41	41	99.99899932

42	42	99.99899932
43	43	99.99899932
44	15	0

The table above includes both the real and the predicted faulted nodes. On inspection, the majority of estimates are correct. With respect to estimation likelihoods, most values once again surpass 99.95%. Aggregating the results, this scenario reports the following.

- The average estimation probability is 68.60%.
- Correct estimations account for 72.09% of the total.

In this case, there is a total of 12 incorrect estimations. However, the errors in this instance are of a different nature than those of the past scenario. Table 13 shows incorrect predictions on several nodes. In all those cases, the estimated location was only one node away from the faulty node. This means that, while the average estimation likelihood is 68.60%, the errors in prediction are relatively small when compared to the past errors.

When computed, the distance between the faulty node and the estimated node is shown in Table 13.

Table 12. Error distances (km)

<i>Faulty Node</i>	<i>Final Estimated Node</i>	<i>Distance to Fault (km)</i>
17	18	0.146
21	22	0.537
22	23	0.09
25	26	0.347
26	27	0.102
29	30	0.2
33	34	0.165

34	35	0.081
35	36	0.065
38	11	0.209
39	12	0.1
44	15	2.379

This yields a mean distance of 10.53m between the estimated fault and the actual fault across the entire network. When contrasted with the grid's geographical extent, this figure amounts to 1.27%. In other words, the method produces estimates with an average error of 1.27% of the analysed network.

Still, the fault in node 37 is not detected by the algorithm, and fault node 44 is still mistakenly predicted at node 15.

To summarise, this scenario produced the following results.

- The method presents an average estimation probability of 68.60%.
- A total of 72.09% of the estimations were correct.

5.2 DISCUSSION

5.2.1 OVERALL BEHAVIOUR

The final results of this study are shown in this section, as well as the general discussion regarding them. Here are tables, graphs, and figures explaining the results and comparing them with the expected outcomes.

Once all results are considered together, the pattern becomes easier to see. Figure 7 presents the average estimation probability for the three fault types across the three-fault resistance (FR) levels. A consistent tendency appears, as FR increases, the mean estimation probability tends to drop. This behaviour was expected and is visible in the figure for all three fault categories, where the estimation values decline as the FR moves from 0Ω to 1Ω to 5Ω .

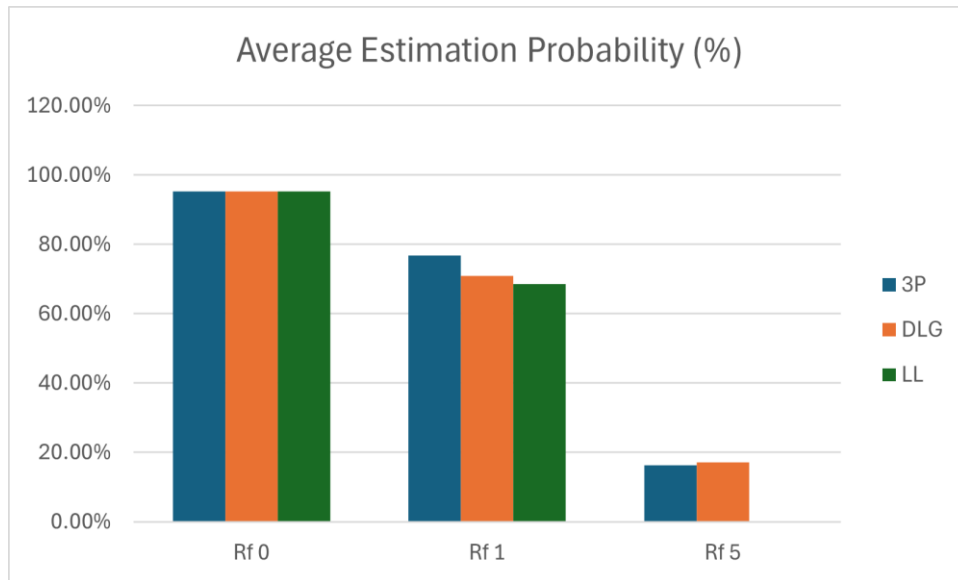


Figure 7. Average Estimation Probability (%)

Estimation probability alone, however, does not fully describe the method's behaviour. A second viewpoint is needed for this. Figure 8 reports the percentage of correct estimations for each scenario in the analysed grid. The numbers closely track those in the previous figure, which is reasonable because most correct classifications carry probabilities very close to 100

percent. As a result, the average probability and the share of correct outcomes move in parallel.

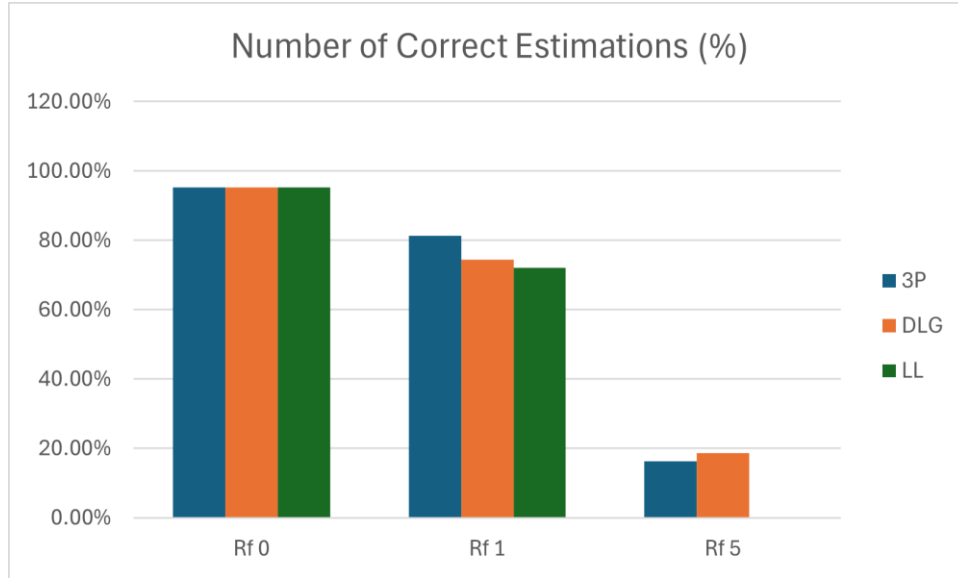


Figure 8. Number of Correct Estimations (%)

It is also clear that the predictions obtained with an FR of 5Ω show lower probabilities and reduced accuracy. Yet this count of correct cases relies on a binary decision: either the estimate matches the true node, or it does not. To better interpret the results, it is necessary to add a measure that reflects how far a wrong estimate is from the actual faulted section.

Figure 9 offers that perspective by plotting the distance between the node predicted by the algorithm and the true location. This view helps to judge the severity of errors rather than only their occurrence. The pattern is straightforward, low FR values lead to small distances. More interestingly, the 5Ω scenarios still produce an average spatial error of about 3.2 % of the grid's extent, which is not especially large. This reframes the earlier accuracy figures and provides a more balanced view of performance under higher resistance.

The reason for the degradation at 5Ω is consistent with the theory of single-ended, impedance-based location. The additional voltage drop across the fault resistance is interpreted as part of the line, so the apparent impedance becomes the sum of the true line

segment and a term that scales with FR and the fault type. If the model is tuned around lower FR, that extra drop is read as extra distance, creating a bias that grows with resistance. A higher FR also lowers fault current, reducing the contrast between pre-fault and fault phasors; residual load components, infeed, and modest measurement errors therefore matter more. For ground faults, zero-sequence paths and grounding impedances can further disturb

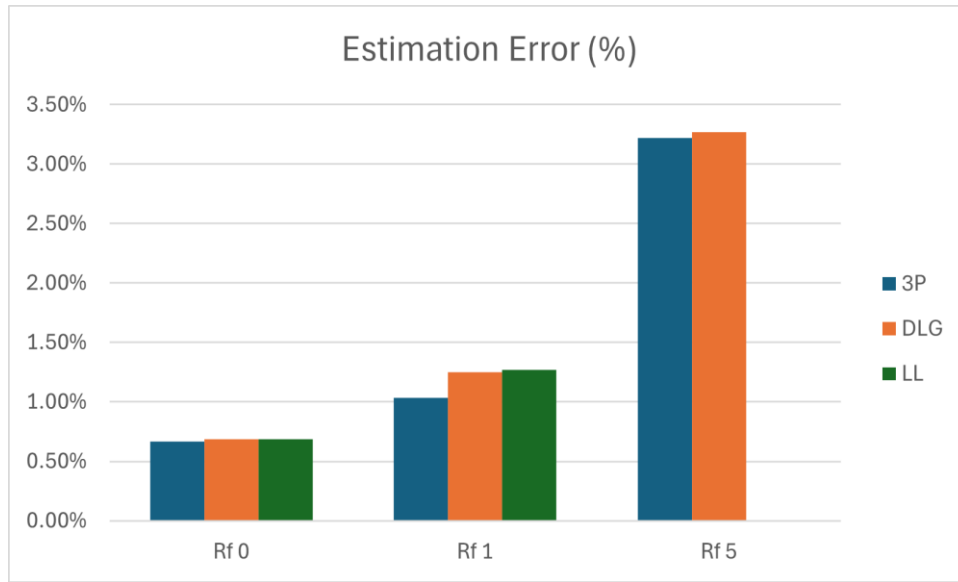


Figure 9. Estimation Error Distance (%)

simplified positive-sequence assumptions and add to the error.

Even so, the 5Ω simulations in this study do not show extreme deviations. Three factors likely explain this outcome.

First, the phasors are clean, and parameters are well specified, which reduces noise that would otherwise magnify high-resistance effects. Third, the approach combines viewpoints from multiple PMUs, this means that weaker estimates lose weight when results are fused, and the final location tends to be pulled toward the more reliable predictions.

Taken together, these observations suggest that FR is more impactful in performance than fault type. In practical terms, the method behaves consistently across the three fault categories as long as the resistance level remains comparable.

5.2.2 COMPARISON VS. BASELINE CASE

All these results are interesting on their own, but the value of the obtained outcomes does not only rely on their isolated values, but also on their performance when compared to other methods' results. In an effort to further visualise these methods' accuracy, the obtained data is compared to a baseline in this section.

The algorithm computes its estimations based on the data obtained from each one of the measurement points in the grid and then combines six different estimation data sets to end up with only one set of estimation data. This baseline case relies on a single measurement point at the head of the grid and instead of combining the resulting predictions with others, it estimates based solely on that one set of information. Naturally, this will mean that the amount of information with which the algorithm uses to produce a prediction is less than this study's case, and thus it is expected to have a lower accuracy and higher error ratio.

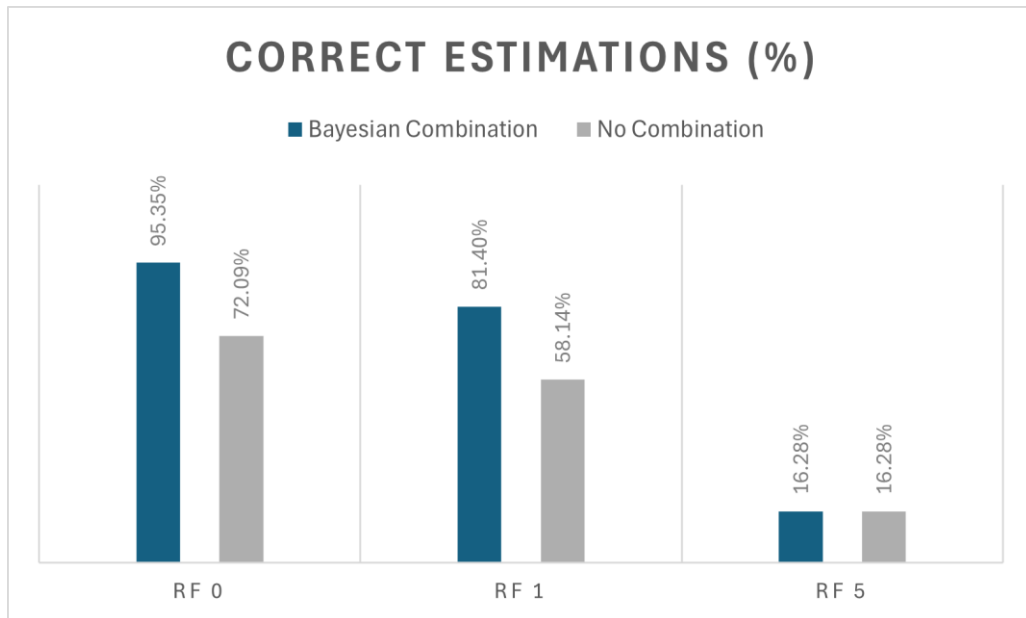


Figure 10. Percentage of Correct Estimations.

When set against the Bayesian combination, it can be seen that the baseline accuracy is smaller, the correct classification rate decreases by about 23.26% in FR 0Ω and 1Ω scenarios, from 95.35% to 72.09% for 0Ω and from 81.40% to 58.14% for 1Ω , while the third FR scenario presents only a small difference in value. This is all visible in Figure 10.

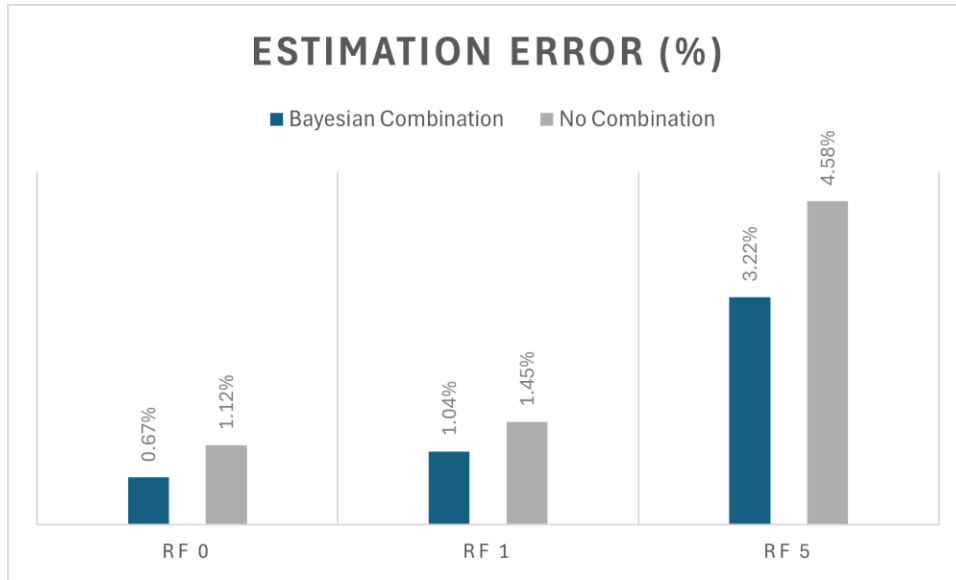


Figure 11. Distance to Actual Fault (%).

Several factors are likely to contribute to this gap. Firstly, a head-end point of view offers limited visibility of deep feeder sections, as the fault lies farther from the substation, the distinctiveness of the measured phasors is decreased. Also, with higher fault resistances, the extra voltage drop across the fault is read by the estimator as additional line length, which biases the apparent impedance even further, which is visible in Figure 11.

From an operational perspective, the differences are modest but not trivial. A reduction in correct identifications implies more switching steps or extra field checks before location, while the added distance error translates into longer patrol distance. Where the infrastructure supports multiple PMUs, the Bayesian fusion is preferable. If only a head-end PMU is available, the baseline still offers a somewhat decent performance, but its limitations should be expected to increase in high-resistance scenarios. Future work could examine whether

lightweight compensation for fault resistance, or adaptive reweighting of PMUs based on past performance, narrows the remaining gap without adding significant complexity.

The Bayesian combination of different probabilities proves useful to increase the certainty of a fault being in a certain location. Each individual measurement point, whether it is PMU or not, is capable of delivering a limited certainty that a fault is located in any given portion of the grid. The Bayesian consideration of previous probability helps this “current probability” increase with any extra information that can be extracted from the scenario and ultimately increases the overall probability and therefore, the accuracy of this method.

In this study, the Bayesian comparison yields a 32.25% improvement in estimation capability for FR 0 scenarios and a 32.98% improvement for FR 1 scenarios. Taken together with the distance results, these gains support the use of multi-point fusion for location in the analysed grid, while also indicating where further refinement should focus.

Chapter 6. CONCLUSIONS AND FUTURE WORK

This project set out to improve fault location in medium-voltage distribution networks while keeping deployment costs realistic. The method combines a single-ended impedance estimator with a Bayesian step that combines several perspectives, prioritising PMU placements that coincide with existing measurement sites to limit new infrastructure. The broader motivation of the study is quality of service (QOS), a faster and more reliable location shortens isolation and restoration, which supports continuity for customers and safer operations.

Methodologically, the work proceeds along two tracks. First, it builds a reproducible pipeline that ingests event waveforms, forms phasors, computes apparent impedances, and maps these to likely positions along the feeder. Second, it merges per-sensor outputs into a single posterior using Bayes' theorem with simple priors. The case study is a 43-node urban feeder in Milan, chosen to keep analysis tractable while retaining realistic features such as branching laterals and varied sequence parameters. PMUs are assumed at legacy monitor sites so the study can ask not only whether accuracy improves, but whether the gains arise in a way a DSO could plausibly adopt.

Across nine scenario families that cross three fault types with three resistance levels, three patterns emerge. At low fault resistance the method performs well, in several 0 Ω cases correctly identifying most events with high posterior probabilities. As resistance increases, accuracy declines, which aligns with single-ended impedance theory because the extra drop across the fault is interpreted as additional line length. Even so, at 5 Ω the distance errors remain moderate: the average error is close to three per cent of the grid's extent, which keeps switching and patrol effort local rather than feeder-wide.

In this case, the distance matters because a simple judgement whether its estimation is correct or not does not convey how far a wrong estimate lies from the true section. The distance metric contextualizes these results. Low resistances cause small deviations, and a higher resistance, while it lowers the number of correct estimations, still produces errors that cluster

near the correct area. This means that even though higher resistance levels may cause the estimations to be incorrect, estimated locations do not fall far away from the faulty section. With this, it can be expected that this method degrades in a controlled manner under added resistance, which is precisely the condition that often complicates field work.

To reinforce this analysis, a structured comparison with a single-sensor baseline is carried out. Relying only on the head-end viewpoint reduces observability of deeper feeder sections. In the results, correct classifications fall by roughly 32% in the 0 Ω and 1 Ω groups, and distance errors rise slightly. This is consistent with local bias from branching, infeed, and resistance-induced drops that the single point reads as extra length. Fusion reduces the impact of these effects by reducing weak perspectives and concentrating probability on candidates supported by multiple sensors.

Additionally, the deployment implications are considered. Reusing existing sites is a pragmatic compromise between ideal placement and cost. This decision facilitates implementation and eases smart grid modernisation.

However, the algorithm presents a key limitation. The header measurement device has weaker synchronisation than PMU-grade points, which is detrimental to the results when that perspective dominates. PMU installation on the header of the grid is not yet technologically feasible, which limits options to counter this problem. Even then, the potential affected estimations would be located closer to the header, which helps mitigate any inaccuracies.

Even with its limitation, the possible applications are clear. For operators, multi-PMU fusion offers clear improvement over a single sensor, particularly for distant faults and non-negligible resistance. The distance-based view suggests that a small set of well-placed PMUs can shorten patrol lengths and reduce the number of switching steps before isolation. For planners, the results point to incremental deployment tied to legacy sites, and to treating resistance compensation and calibration as first-order concerns.

The work also identifies concrete next steps. Modest fault-resistance compensation inside the estimator, tuned to local parameters, could reduce bias that grows with resistance.

Relaxing the independence assumption during fusion, through covariance-aware weighting or learning sensor reliability from past events, may help. Testing resilience under noise, dropouts, and timestamp jitter, together with ablations that remove individual PMUs to measure marginal value, would further clarify applicability.

In summary, a single-ended impedance method, paired with simple probabilistic fusion across a handful of strategically located sensors, can provide accurate and operationally useful fault locations on an urban MV feeder. Although performance falls with increasing resistance, spatial errors remain contained, and fusion outperforms a single head-end baseline by a meaningful margin. The combination of practical placement, transparent computation, and clear reporting offers a credible path from study to deployment, and a foundation for incremental refinements that target the most consequential sources of error.

Chapter 7. BIBLIOGRAPHY

- [1] D. and I. S. Banerjee Binayak and Jayaweera, "Fundamentals of Power Systems," in *Smart Power Systems and Renewable Energy System Integration*, D. Jayaweera, Ed., Cham: Springer International Publishing, 2016, pp. 1–13. doi: 10.1007/978-3-319-30427-4_1.
- [2] A. G. Phadke, M. Ibrahim and T. Hlibka, "Fundamental basis for distance relaying with symmetrical components," in *IEEE Transactions on Power Apparatus and Systems*, vol. 96, no. 2, pp. 635–646, March 1977, doi: 10.1109/T-PAS.1977.32375.
- [3] S. S. Yu, Md. S. Rahman, G. Zhang, S. T. Meraj, and H. Trinh, "Comprehensive review of PMU applications in smart grid: Enhancing grid reliability and efficiency," *Chinese Journal of Electrical Engineering*, pp. 1–41, 2025, doi: 10.23919/CJEE.2025.000129.
- [4] T. S. Menezes, P. H. A. Barra, F. A. S. Dizioli, V. A. Lacerda, R. A. S. Fernandes, and D. v. Coury, "A Survey on the Application of Phasor Measurement Units to the Protection of Transmission and Smart Distribution Systems," *Electric Power Components and Systems*, vol. 52, no. 8, pp. 1379–1396, 2024, doi: 10.1080/15325008.2023.2240320.
- [5] "IEEE Guide for Determining Fault Location on AC Transmission and Distribution Lines," in *IEEE Std C37.114-2004*, vol., no., pp.1-44, 8 June 2005, doi: 10.1109/IEEESTD.2005.96207.
- [6] J. R. Carson, "Wave propagation in overhead wires with ground return," *The Bell System Technical Journal*, vol. 5, no. 4, pp. 539–554, 1926, doi: 10.1002/j.1538-7305.1926.tb00122.x.
- [7] S. Marx, B. P. Administration, B. K. Johnson, A. Guzmán, V. Skendzic, and M. v Mynam, "Traveling Wave Fault Location in Protective Relays: Design, Testing, and Results."
- [8] S. Das, S. Santoso, A. Gaikwad, and M. Patel, "Impedance-based fault location in transmission networks: Theory and application," *IEEE Access*, vol. 2, pp. 537–557, 2014, doi: 10.1109/ACCESS.2014.2323353.
- [9] H. Mirshekali, R. Dashti and H. R. Shaker, "A Novel Fault Location Algorithm for Electrical Networks Considering Distributed Line Model and Distributed Generation Resources," 2020 IEEE PES Innovative Smart Grid Technologies Europe (ISGT-Europe), The Hague, Netherlands, 2020, pp. 16-20, doi: 10.1109/ISGT-Europe47291.2020.9248755.
- [10] K. Zhuang, S. Mou, H. Chen, M. Cui, and L. Wang, "A Fault Location Method for Modern Distribution Network Based on Fault State Estimation by Hybrid Measurement," in *2024 8th*

- International Conference on Smart Grid and Smart Cities, ICSGSC 2024*, Institute of Electrical and Electronics Engineers Inc., 2024, pp. 141–146. doi: 10.1109/ICSGSC62639.2024.10813844.
- [11] H. Mirshekali, R. Dashti, A. Keshavarz, and H. R. Shaker, “Machine Learning-Based Fault Location for Smart Distribution Networks Equipped with Micro-PMU,” *Sensors*, vol. 22, no. 3, Feb. 2022, doi: 10.3390/s22030945.
- [12] A. Pal, A. K. S. Vullikanti and S. S. Ravi, "A PMU Placement Scheme Considering Realistic Costs and Modern Trends in Relaying," in *IEEE Transactions on Power Systems*, vol. 32, no. 1, pp. 552-561, Jan. 2017, doi: 10.1109/TPWRS.2016.2551320.
- [13] U.S. Department of Energy, Electricity Delivery and Reliability, “Synchrophasor technologies and their deployment in the recovery act smart grid programs,” Aug. 2013. [Online]. Available: <http://energy.gov/sites/prod/files/2013/08/f2/SynchrophasorRptAug2013.pdf>
- [14] Cruz, Marco & Rocha, Helder & Paiva, Marcia & Segatto, Marcelo & Camby, Eglantine & Caporossi, Gilles. (2019). An algorithm for cost optimization of PMU and communication infrastructure in WAMS. *International Journal of Electrical Power & Energy Systems*. 106. 96-104. 10.1016/j.ijepes.2018.09.020.
- [15] P. System Relaying Committee of the IEEE Power and E. Society, “IEEE Standard for Synchrophasor Measurements for Power Systems Sponsored by the Power System Relaying Committee IEEE Power & Energy Society,” 2011.
- [16] I. Power, E. Society, and P. System Relaying, *INTERNATIONAL STANDARD Measuring relays and protection equipment-Part 118-1: Synchrophasor for power systems-Measurements*. 2018.
- [17] M. S. Turiman, M. K. N. M. Sarmin, N. Saadun, L. C. Chong, H. Ali, and Q. Mohammad, “Analysis of High Penetration Level of Distributed Generation at Medium Voltage Levels of Distribution Networks,” in *2022 IEEE International Conference on Power Systems Technology: Embracing Advanced Technology in Power and Energy Systems for Sustainable Development, POWERCON 2022*, Institute of Electrical and Electronics Engineers Inc., 2022. doi: 10.1109/POWERCON53406.2022.9929780.
- [18] A. Harb, W. A. Saliek, and M. Alhusseini, “On the Impacts of Renewable Energy on Distribution Power Systems and the Effects of Energy Storage Systems,” in *2023 14th International Renewable Energy Congress, IREC 2023*, Institute of Electrical and Electronics Engineers Inc., 2023. doi: 10.1109/IREC59750.2023.10389307.

- [19] J. O. Petinrin and M. Shaabanb, "Impact of renewable generation on voltage control in distribution systems," *Renewable and Sustainable Energy Reviews*, vol. 65, pp. 770–783, Nov. 2016, doi: 10.1016/J.RSER.2016.06.073.
- [20] K. Kaushal, P. Syal, and S. K. Sinha, "A Brief Study on Optimal Placement of Phasor Measurement Unit," in *2018 3rd International Innovative Applications of Computational Intelligence on Power, Energy and Controls with their Impact on Humanity (CIPECH)*, 2018, pp. 215–220. doi: 10.1109/CIPECH.2018.8724316.
- [21] United Nations, "The 2030 Agenda for Sustainable Development's 17 Sustainable Development Goals (SDGs).", 4th SDG Youth Summer Camp – SDG Resource Document, 2020.
- [22] A. G. Phadke and J. S. Thorp, "HISTORY AND APPLICATIONS OF PHASOR MEASUREMENTS," 2006 IEEE PES Power Systems Conference and Exposition, Atlanta, GA, USA, 2006, pp. 331-335, doi: 10.1109/PSCE.2006.296328.
- [23] C. E. Ogbogu, J. Thornburg, and S. O. Okozi, "Smart Grid Fault Mitigation and Cybersecurity with Wide-Area Measurement Systems: A Review," *Energies*, vol. 18, no. 4. Multidisciplinary Digital Publishing Institute (MDPI), Feb. 01, 2025. doi: 10.3390/en18040994.
- [24] A. Chandra, G. K. Singh, and V. Pant, "Protection of AC microgrid integrated with renewable energy sources – A research review and future trends," *Electric Power Systems Research*, vol. 193, p. 107036, Apr. 2021, doi: 10.1016/J.EPSR.2021.107036.
- [25] M. Hojabri, U. Dersch, A. Papaemmanouil, and P. Bosshart, "A comprehensive survey on phasor measurement unit applications in distribution systems," *Energies*, vol. 12, no. 23. MDPI AG, Nov. 29, 2019. doi: 10.3390/en12234552.
- [26] M. M. Ahmed, M. Amjad, M. A. Qureshi, K. Imran, Z. M. Haider, and M. O. Khan, "A Critical Review of State-of-the-Art Optimal PMU Placement Techniques," *Energies*, vol. 15, no. 6, Mar. 2022, doi: 10.3390/en15062125.
- [27] A. Pazderin *et al.*, "Directions of Application of Phasor Measurement Units for Control and Monitoring of Modern Power Systems: A State-of-the-Art Review," *Energies*, vol. 16, no. 17. Multidisciplinary Digital Publishing Institute (MDPI), Sep. 01, 2023. doi: 10.3390/en16176203.
- [28] C. E. Ogbogu, J. Thornburg, and S. O. Okozi, "Smart Grid Fault Mitigation and Cybersecurity with Wide-Area Measurement Systems: A Review," *Energies*, vol. 18, no. 4. Multidisciplinary Digital Publishing Institute (MDPI), Feb. 01, 2025. doi: 10.3390/en18040994.

- [29] S. S. Yu, Md. S. Rahman, G. Zhang, S. T. Meraj, and H. Trinh, "Comprehensive review of PMU applications in smart grid: Enhancing grid reliability and efficiency," *Chinese Journal of Electrical Engineering*, pp. 1–41, 2025, doi: 10.23919/CJEE.2025.000129.
- [30] D. Passos, C. de Sousa, R. C. Gomes, D. F. Assis, F. G. O. Passos, and C. Albuquerque, "A Tutorial and Security Overview on the IEEE 2030.5-2018 Standard," *IEEE Communications Surveys and Tutorials*. Institute of Electrical and Electronics Engineers Inc., 2025. doi: 10.1109/COMST.2025.3532110.
- [31] S. Sundarajoo and D. M. Soomro, "Under voltage load shedding and penetration of renewable energy sources in distribution systems: a review," *International Journal of Modelling and Simulation*, vol. 43, no. 6, pp. 1002–1020, 2023, doi: 10.1080/02286203.2022.2143191.
- [32] A. Chandra, G. K. Singh, and V. Pant, "Protection of AC microgrid integrated with renewable energy sources – A research review and future trends," *Electric Power Systems Research*, vol. 193, p. 107036, Apr. 2021, doi: 10.1016/J.EPSR.2021.107036.
- [33] G. P. Reddy and Y. v. Pavan Kumar, "Smart grid communication and networking: Review of standards," in *2021 International Conference on Applied and Theoretical Electricity, ICATE 2021 - Proceedings*, Institute of Electrical and Electronics Engineers Inc., May 2021. doi: 10.1109/ICATE49685.2021.9465005.
- [34] A. E. Saldaña-González, A. Sumper, M. Aragüés-Peñalba, and M. Smolnikar, "Advanced distribution measurement technologies and data applications for smart grids: A review," *Energies*, vol. 13, no. 14. MDPI AG, Jul. 01, 2020. doi: 10.3390/en13143730.
- [35] M. Sefid and M. Rihan, "Optimal PMU placement in a smart grid: An updated review," *International Journal of Smart Grid and Clean Energy*, vol. 8, no. 1, pp. 59–69, Jan. 2019, doi: 10.12720/sgce.8.1.59-69.
- [36] A. Sundararajan, T. Khan, A. Moghadasi, and A. I. Sarwat, "Survey on synchrophasor data quality and cybersecurity challenges, and evaluation of their interdependencies," *Journal of Modern Power Systems and Clean Energy*, vol. 7, no. 3. Springer Heidelberg, pp. 449–467, May 01, 2019. doi: 10.1007/s40565-018-0473-6.
- [37] S. Kakran and S. Chanana, "Smart operations of smart grids integrated with distributed generation: A review," *Renewable and Sustainable Energy Reviews*, vol. 81. Elsevier Ltd, pp. 524–535, 2018. doi: 10.1016/j.rser.2017.07.045.
- [38] P. Roy, S. Bhattacharjee, S. Abedzadeh, and S. K. Das, "Noise Resilient Learning for Attack Detection in Smart Grid PMU Infrastructure," *IEEE Transactions on Dependable and Secure Computing*, pp. 1–17, Jan. 2022, doi: 10.1109/tdsc.2022.3223288.

- [39] R. Setola, G. Oliva, G. Assenza, and L. Faramondi, "Cyber Threats for Operational Technologies", doi: 10.1504/ijss.2020.109127.
- [40] A. Bayat, A. Bagheri, and R. B. Navesi, "A real-time PMU-based optimal operation strategy for active and reactive power sources in smart distribution systems," *Electric Power Systems Research*, vol. 225, Dec. 2023, doi: 10.1016/j.epsr.2023.109842.
- [41] M. Pignati, L. Zanni, P. Romano, R. Cherkaoui, and M. Paolone, "Fault Detection and Faulted Line Identification in Active Distribution Networks Using Synchrophasors-Based Real-Time State Estimation," *IEEE Transactions on Power Delivery*, vol. 32, no. 1, pp. 381–392, Feb. 2017, doi: 10.1109/TPWRD.2016.2545923.
- [42] P. A. Pegoraro, C. Sitzia, A. V. Solinas, S. Sulis, D. Carta, and A. Benigni, "Compensation of Systematic Errors for Improved PMU-based Fault Detection and Location in Three-Phase Distribution Grids," *IEEE Transactions on Instrumentation and Measurement*, 2024, doi: 10.1109/TIM.2024.3400340.
- [43] P. Ray and S. Beura, "Accurate Fault Detection of Distribution Network with Optimal Placement of Phasor Measurement Unit," 2019 International Conference on Intelligent Sustainable Systems (ICISS), Palladam, India, 2019, pp. 76-81, doi: 10.1109/ISS1.2019.8908029.
- [44] M. Gholami, A. Abbaspour, M. Moeini-Aghaie, M. Fotuhi-Firuzabad and M. Lehtonen, "Detecting the Location of Short-Circuit Faults in Active Distribution Network Using PMU-Based State Estimation," in *IEEE Transactions on Smart Grid*, vol. 11, no. 2, pp. 1396-1406, March 2020, doi: 10.1109/TSG.2019.2937944.
- [45] K. Kaushal, P. Syal and S. K. Sinha, "A Brief Study on Optimal Placement of Phasor Measurement Unit," 2018 3rd International Innovative Applications of Computational Intelligence on Power, Energy and Controls with their Impact on Humanity (CIPECH), Ghaziabad, India, 2018, pp. 215-220, doi: 10.1109/CIPECH.2018.8724316.
- [46] V. S. K. V. Harish, S. Gupta, J. G. Bhatt, and M. Bansal, "International standards, regulations, and best practices for cyber security of smart grid," *Cyber Security Solutions for Protecting and Building the Future Smart Grid*, pp. 321–348, Jan. 2025, doi: 10.1016/B978-0-443-14066-2.00010-4.
- [47] I. E. Ivanov, Y. A. Umnov, A. A. Yablokov, and A. R. Tychkin, "Comparison of transmission line parameter estimation algorithms through simulated and real-field PMU data," in *International Youth Conference on Radio Electronics, Electrical and Power Engineering, REEPE*, Institute of Electrical and Electronics Engineers Inc., 2025. doi: 10.1109/REEPE63962.2025.10971101.

- [48] P. A. Pegoraro, C. Sitzia, A. V. Solinas, S. Sulis, D. Carta, and A. Benigni, "Improved Fault Detection and Location Method in Three-Phase Distribution Networks Leveraging Traceable PMU Measurements," *IEEE Transactions on Instrumentation and Measurement*, vol. 74, 2025, doi: 10.1109/TIM.2025.3561427.
- [49] P. A. Pegoraro, C. Sitzia, A. V. Solinas, S. Sulis, D. Carta, and A. Benigni, "Fault Identification Method in Three-Phase Distribution Networks Leveraging Traceable PMU Measurements," in *2024 14th IEEE International Workshop on Applied Measurements for Power Systems, AMPS 2024 - Proceedings*, Institute of Electrical and Electronics Engineers Inc., 2024. doi: 10.1109/AMPS62611.2024.10706699.
- [50] H. M. Khalid, F. Flitti, M. S. Mahmoud, M. M. Hamdan, S. M. Muyeen, and Z. Y. Dong, "Wide area monitoring system operations in modern power grids: A median regression function-based state estimation approach towards cyber attacks," *Sustainable Energy, Grids and Networks*, vol. 34, Jun. 2023, doi: 10.1016/j.segan.2023.101009.
- [51] A. Pazderin *et al.*, "Directions of Application of Phasor Measurement Units for Control and Monitoring of Modern Power Systems: A State-of-the-Art Review," *Energies*, vol. 16, no. 17. Multidisciplinary Digital Publishing Institute (MDPI), Sep. 01, 2023. doi: 10.3390/en16176203.
- [52] R. L. A. Reis *et al.*, "Evaluation of single-ended impedance-based transmission fault location using fixed and variable window phasor estimation approaches," *Electric Power Systems Research*, vol. 223, p. 109571, Oct. 2023, doi: 10.1016/J.EPSR.2023.109571.
- [53] N. M. Tawfik, N. H. El-Amary, and L. Nasrat, "Phasor Measurement Unit Optimal Allocation Utilizing Discrete Water Cycle Optimization," in *Proceedings of the 2023 5th International Youth Conference on Radio Electronics, Electrical and Power Engineering, REEPE 2023*, Institute of Electrical and Electronics Engineers Inc., 2023. doi: 10.1109/REEPE57272.2023.10086708.
- [54] S. H. Hosseini Dolatabadi and M. E. Hamedani Golshan, "Fault location observability rules for impedance-based fault location algorithms," *Electric Power Systems Research*, vol. 224, Nov. 2023, doi: 10.1016/j.epsr.2023.109771.
- [55] P. H. Nguyen and H. G. Vu, "Operation Schemes of Medium Voltage Distribution Networks with High Penetration of Distributed Solar Photovoltaics," in *Conference Proceedings - 2023 IEEE Asia Meeting on Environment and Electrical Engineering, EEE-AM 2023*, Institute of Electrical and Electronics Engineers Inc., 2023. doi: 10.1109/EEE-AM58328.2023.10395035.
- [56] O. Tshenyego, R. Samikannu, B. Mtengi, M. Mosalaosi, and T. Sigwele, "A Graph-Theoretic Approach for Optimal Phasor Measurement Units Placement Using Binary Firefly Algorithm," *Energies*, vol. 16, no. 18, Sep. 2023, doi: 10.3390/en16186550.

- [57] M. M. Ahmed, M. Amjad, M. A. Qureshi, K. Imran, Z. M. Haider, and M. O. Khan, "A Critical Review of State-of-the-Art Optimal PMU Placement Techniques," *Energies*, vol. 15, no. 6, Mar. 2022, doi: 10.3390/en15062125.
- [58] H. J. Lee, C. Qin, and A. K. Srivastava, "Adaptive Phasor Estimation for Smart Electric Grid Monitoring Applications," in *Conference Record - IAS Annual Meeting (IEEE Industry Applications Society)*, Institute of Electrical and Electronics Engineers Inc., 2022. doi: 10.1109/IAS54023.2022.9939979.
- [59] R. Bhargav, C. P. Gupta, and B. R. Bhalja, "Unified Impedance-Based Relaying Scheme for the Protection of Hybrid AC/DC Microgrid," *IEEE Transactions on Smart Grid*, vol. 13, no. 2, pp. 913–927, Mar. 2022, doi: 10.1109/TSG.2021.3129532.
- [60] J. J. Chavez *et al.*, "PMU-voltage drop based fault locator for transmission backup protection," *Electric Power Systems Research*, vol. 196, Jul. 2021, doi: 10.1016/j.epsr.2021.107188.
- [61] C. Fang, Z. Shi, Y. Peng, Z. Wu, W. Gu, and P. Nie, "Fault Location in Distribution Networks Using PMU Data and Interval Algorithm," in *2019 9th International Conference on Power and Energy Systems (ICPES)*, 2019, pp. 1–6. doi: 10.1109/ICPES47639.2019.9105381.
- [62] M. A. R. S. Cruz, H. R. O. Rocha, M. H. M. Paiva, M. E. V. Segatto, E. Camby, and G. Caporossi, "An algorithm for cost optimization of PMU and communication infrastructure in WAMS," *International Journal of Electrical Power and Energy Systems*, vol. 106, pp. 96–104, Mar. 2019, doi: 10.1016/j.ijepes.2018.09.020.
- [63] S. S. Mousavi-Seyedi, F. Aminifar, M. R. Rezaei, and R. Hasani, "Optimal fault location algorithm for series-compensated transmission lines based on PMU data," in *2015 Smart Grid Conference (SGC)*, 2015, pp. 105–109. doi: 10.1109/SGC.2015.7857418.
- [64] F. Aminifar, M. Fotuhi-Firuzabad, A. Safdarian, A. Davoudi, and M. Shahidehpour, "Synchrophasor Measurement Technology in Power Systems: Panorama and State-of-the-Art," *IEEE Access*, vol. 2, pp. 1607–1628, 2014, doi: 10.1109/ACCESS.2015.2389659.
- [65] S. Das, N. Karnik, and S. Santoso, "Distribution fault-locating algorithms using current only," *IEEE Transactions on Power Delivery*, vol. 27, no. 3, pp. 1144–1153, 2012, doi: 10.1109/TPWRD.2012.2191422.
- [66] Z. Radojević and V. Terzija, "Effective two-terminal numerical algorithm for overhead lines protection," *Electrical Engineering*, vol. 89, no. 5, pp. 425–432, May 2007, doi: 10.1007/s00202-006-0014-6.

- [67] Z. Radojević and V. Terzija, "Numerical algorithm for overhead lines protection and disturbance records analysis," *IET Generation, Transmission and Distribution*, vol. 1, no. 2, pp. 357–363, 2007, doi: 10.1049/iet-gtd:20060139.
- [68] K. Zimmerman and D. Costello, "Impedance-Based Fault Location Experience," in *2006 IEEE Rural Electric Power Conference*, 2006, pp. 1–16. doi: 10.1109/REPCON.2006.1649060.
- [69] A. S. A. Awad, D. Turcotte, and T. H. M. El-Fouly, "Impact Assessment and Mitigation Techniques for High Penetration Levels of Renewable Energy Sources in Distribution Networks: Voltage-control Perspective," *Journal of Modern Power Systems and Clean Energy*, vol. 10, no. 2, pp. 450–458, Mar. 2022, doi: 10.35833/MPCE.2020.000177.

Chapter 8. ANNEXES

8.1 ANNEX A: SOURCE CODE

8.1.1 MAIN SCRIPT

```
clc
clear
close all

%%
%GET HV DATA
run("get_HV_data.m");
load("HV_data.mat");
Vn=str2double(HV_data(2,6))*1000;

fprintf('V2n TRASF: %f [V]\n',Vn);

%%
%GET FEEDER
load("grid.mat");
load("G.mat");
load("nodes.mat");

%% CSV Data
% Select Folder containing all PMU-specific CSV Fault Files
fault_data_folder = uigetdir('', 'Select Folder Containing ALL CSV Fault Data Files (e.g., PMU1_NodeX_TypeY.csv)');
if isequal(fault_data_folder, 0)
    error('Fault data folder selection cancelled. Cannot proceed.');
```

```
end
fprintf('Selected Fault Data Folder: %s\n', fault_data_folder);

% Get a list of all CSV files in the selected folder
all_csv_files = dir(fullfile(fault_data_folder, '*.csv'));

if isempty(all_csv_files)
    error('No CSV files found in the selected folder.');
```

```
end
fprintf('Found %d CSV fault data files in total.\n', length(all_csv_files));

for k = 1:length(all_csv_files)
    current_filename = all_csv_files(k).name;

    % This regex expects a format like 'PMU[ID]_[SCENARIO_KEY].csv'
    % tokens = regexp(current_filename,
    'A85(\d+)_PMU(\d+)_(Node\d+.*?)_3PRf(\d+)\.csv', 'tokens', 'once');
```

```

tokens = regexp(current_filename, 'A(.*)_PMU(.*)_(.*)_Rf_(\d+)\.csv$',
'tokens', 'once');
if isempty(tokens)
    warning('Filename does not match expected pattern (PMU[X]_Node[NN]...).'
Skipping: %s', current_filename);
    continue;
end
tokenmat(k,:)=tokens;
tokenvec(k,1)=string(current_filename);
pmu_id_num = str2double(tokens{2}); % e.g., 1, 2, 3, 4
scenario_key = current_filename; % e.g., "Node45_3P_Rf0_A12345"
myTable(k,:) = table(string(tokenmat(k,1)), string(tokenmat(k,2)),
string(tokenmat(k,3)), string(tokenmat(k,4)), ...
    'VariableNames', {'NodeCode', 'PMU', 'FaultType', 'Rf'});
end

%% Main
Location_Probability = zeros(height(nodes),height(all_csv_files));
epsilon = 1e-3; % A very small constant to avoid absolute zeros

full_rtds_filepath = fullfile(fault_data_folder,tokenvec);

h = waitbar(0, 'Please wait...', 'Fault Location', 'Current progress');
for k = 1:length(all_csv_files)
    current_fraction = k/length(all_csv_files);
    waitbar(current_fraction, h, sprintf('Processing %.f%% . . .',
100*k/length(all_csv_files)));
    if str2double(tokenmat(k,2)) == 1
        PMU_node = 1;
    elseif string(tokenmat{k,2}) == '2A' || string(tokens{1,2}) == '2B'
        PMU_node = 10;
    elseif str2double(tokenmat(k,2)) == 3
        PMU_node = 20;
    elseif str2double(tokenmat(k,2)) == 4
        PMU_node = 26;
    elseif str2double(tokenmat(k,2)) == 5
        PMU_node=30;
    end

    waveform=readmatrix(fullfile(full_rtds_filepath(k,1)));

    [MHO_percentage] =
Impedance_method_v4(PMU_node,grid,G,nodes,HV_data,Vn,waveform);

    if myTable.PMU(k) == '2A'
        MHO_percentage(11:37,1)=0;
    elseif myTable.PMU(k) == '2B'
        MHO_percentage(38:44,1)=0;
    end

    % Apply smoothing and convert to probabilities (0-1)

```

```

MHO_percentage_smoothed = (MHO_percentage + epsilon) / 100; % Add epsilon,
then convert to 0-1

Location_Probability(:, k) = MHO_percentage_smoothed;
end
close(h); % Closes the waitbar figure
% end

%% Percentage Combination - Bayes' Theorem
% We must combine the percentages using Bayes' Theorem
Bayesian_Percentage_unnormalized=zeros(height(Location_Probability),1);
Bayesian_Percentage=zeros(height(Location_Probability),1);
Final_Bayesian_Percentage=zeros(height(Location_Probability),1);
for i=1:width(Location_Probability)/6
    % Assuming a uniform prior probability for each node
    prior_probability = ones(height(Location_Probability), 1) /
height(Location_Probability);

    % Element-wise multiplication (equivalent to product if each column is a
likelihood vector)
    % The 'prod' function across the columns will multiply the likelihoods for
each node
    combined_likelihoods = prod(Location_Probability(:,6*i-5:6*i), 2);

    % Calculate the unnormalized posterior
    Bayesian_Percentage_unnormalized(:,i) = combined_likelihoods .*
prior_probability;

    % Normalize to get the final Bayesian posterior probabilities
    Bayesian_Percentage(:,i) =
100*Bayesian_Percentage_unnormalized(:,i)/(sum(Bayesian_Percentage_unnormalized(:,i)));
    %multiplied by 1.0001 to avoid obtaining 100% probabilities
    Final_Bayesian_Percentage(:,i)=Bayesian_Percentage(:,i);
end

%% Plotting
% Assuming you have already run the code to calculate Percentage
C=unique(myTable.NodeCode, 'stable');
% 1. Define Node Numbers
node_numbers = 1:height(Bayesian_Percentage); % Creates a vector [1, 2, ..., 44]
for i=1:width(Final_Bayesian_Percentage)
    % 2. Create the Bar Graph
    % figure; % Opens a new figure window for the plot
    % bar(node_numbers, Final_Bayesian_Percentage(:,i));

    % 3. Label Axes and Title
    % xlabel('Node Number');
    % ylabel('Fault Probability ( )');
    % title('Fault Probability Distribution Across Nodes for Node
'+string(find(C(i,1)==nodes.NomeEnd)));
    % grid on; % Adds a grid for better readability

    % 4. Highlight the Most Probable Node (Optional)

```

```
[max_prob, faulty_node_index] = max(Final_Bayesian_Percentage(:,i));
faulty_node_number = node_numbers(faulty_node_index);

display_Likelihood(i,1)=max_prob;
display_Estimation(i,1)=faulty_node_number;
display_Real(i,1)=find(C(i,1)==nodes.NomeEnd);

% hold on; % Keep the current plot active to add more elements
% text_x_position = faulty_node_number + 2; % Adjust this offset as needed
(e.g., 0.5, 1.0)
% plot(faulty_node_number, max_prob, 'MarkerSize', 12, 'LineWidth', 1.5);
% text(faulty_node_number, max_prob, ...
%     sprintf(' Most Likely Fault: Node %d (%.2f%%)', faulty_node_number,
max_prob), ...
%     'VerticalAlignment', 'baseline', 'HorizontalAlignment', 'left', ...
%     'Color', 'red', 'FontSize', 10);
%
% NodeString=string(find(C(i,1)==nodes.NomeEnd));
% fprintf('Fault is calculated in Node %d with a probability of %.4f%%\n',
faulty_node_number, max_prob);
% fprintf('Fault is actually located in Node %d
\n',find(C(i,1)==nodes.NomeEnd))
End
```

8.1.2 IMPEDANCE METHOD FUNCTION

```
function
[MHO_percentage]=Impedance_method_v4(PMU_node,grid,G,nodes,HV_data,Vn,waveform)

    clc

    %%
    %Z MATRIX
    [Zd, Zo, z_hv, z_hv_0] = get_imped_matrix_v5 (grid,HV_data);

    %%
    %we need to input the data from RTDS

    % waveform=readmatrix(rtds_data);
    % waveform=(waveform);
    % DFT of the PQ waveform
    [E1,E2,E3,Eo_a,Ed_a,Ei_a,I1, I2, I3, Io_a,Id_a,Ii_a] =
DFT_v7(Vn,waveform);

%% Initialize more variables
No_Measure= length(Eo_a(:,1)); %total samples availableN
H = 1;
% frequency=zeros(length(E_MV_busbar(:,1)),2);
```

```
d=0; dl=0;
No_Nodes=height(nodes(:,1));
Zab=zeros(No_Measure-H,2);
Zbc=zeros(No_Measure-H,2);
Zca=zeros(No_Measure-H,2);
fault_type_record=[0,0,0,0,0,0];

%% impedance of the grid seen by each bus (excluding the z_hv)
zd_bus=zeros(No_Nodes,1);
for i=PMU_node:No_Nodes
    zd_bus(i,1)=Zd(i,i)-Zd(PMU_node,PMU_node);
end

%% ALGORITHM STARTS
% Initialize the branch probability method and impedance method

MHO_percentage=zeros(No_Nodes,1);

for i=1:length(Eo_a)

    a=i-H+1;
    Eo = abs(Eo_a(i,2));
    Ed = abs(Ed_a(i,2));
    Ei = abs(Ei_a(i,2));
    Eo_p = angle(Eo_a(i,1));
    Ed_p = angle(Ed_a(i,1));
    Ei_p = angle(Ei_a(i,1));
    Id_p=0;
    Ii_p=0;
    Io_p=0;
    Id=abs(Id_a(i,1));
    Ii=abs(Ii_a(i,1));
    Io=abs(Io_a(i,1));

    % Recall Fault_classifier function
    f_name =
Fault_Classifier(Vn,Ed,Ei,Eo,Ed_p,Ei_p,Eo_p,Id,Ii,Io,Id_p,Ii_p,Io_p);

    % cast of the fault type and isolating the right fault_table part
    switch f_name
        case 'LLL'
            f_type = 1; %3P fault
            fault_type_record(1)=fault_type_record(1)+1;
            j=1:6;
        case 'LL'
            f_type = 2; %LL fault
            fault_type_record(2)=fault_type_record(2)+1;
            j=7:12;
        case 'LG'
            f_type = 3; %SLG fault
            fault_type_record(3)=fault_type_record(3)+1;
            j=13:18;
        case 'LLG'
```



```

        f_type = 4; %DLG fault
        fault_type_record(4)=fault_type_record(4)+1;
        j=19:24;
    case 'No_fault'
        f_type = 5; %NO fault
        fault_type_record(5)=fault_type_record(5)+1;
        j=1:6;
        fprintf('No fault!! \n')
    case 'Error'
        f_type = 6; %Error
        fault_type_record(6)=fault_type_record(6)+1;
        j=1:6;
        fprintf('Error from the fault classifier!! \n')
    end

    % E=
    fault_type(i,1)=f_type;

    if mean(abs(I1)) <501 && mean(abs(I2)) <501 && mean(abs(I3)) <501
        MHO_percentage=zeros(No_Nodes,1);
        return;
    end

    % impedance method_MHO
    if f_type~=0
        Zab(a,1)=(E1(i,1)-E2(i,1))/(I1(i,1)-I2(i,1));
        Zab(a,2)=abs(Zab(a,1));
        Zbc(a,1)=(E2(i,1)-E3(i,1))/(I2(i,1)-I3(i,1));
        Zbc(a,2)=abs(Zbc(a,1));
        Zca(a,1)=(E3(i,1)-E1(i,1))/(I3(i,1)-I1(i,1));
        Zca(a,2)=abs(Zca(a,1));

        % Zab(1:fault_start_idx-1,:)=0;
        % Zbc(1:fault_start_idx-1,:)=0;
        % Zca(1:fault_start_idx-1,:)=0;

        [MHO_ab(:,a),polygon_ab]=Z_map(grid,zd_bus,Zab(a,1));
        [MHO_bc(:,a),polygon_bc]=Z_map(grid,zd_bus,Zbc(a,1));
        [MHO_ca(:,a),polygon_ca]=Z_map(grid,zd_bus,Zca(a,1));

        Za(a,1)=(E1(i,1))/(I1(i,1)); Za(a,2)=abs(Zab(a,1));

        % Filter the fault data

        MHO_ab_result(:,1)=sum(MHO_ab(:,,:),2);
        MHO_bc_result(:,1)=sum(MHO_bc(:,,:),2);
        MHO_ca_result(:,1)=sum(MHO_ca(:,,:),2);

    MHO_result(:,1)=MHO_ab_result(:,1)+MHO_bc_result(:,1)+MHO_ca_result(:,1);

    % The idea is to consider an activation either if there is a
    line-to-line

```

```

% activation or if there is a 3P activation (1 / 3 zones)
answ=MHO_ab(:, :)+MHO_bc(:, :)+MHO_ca(:, :);
cns=round(round(answ./2)./2);
MHO_percentage(:,1)=sum(cns(:, :),2)*100/(No_Measure+H);
% MHO_percentage(:,1)=sum(answ(:, :),2)*100/(sum(MHO_result));
%
MHO_percentage(:,1)=MHO_percentage(:,1)*(sum(MHO_result)/8595);

if sum(MHO_result)==0
    MHO_percentage(:,1)=zeros(height(MHO_percentage),1);
else
    % MHO_percentage(:,1)=MHO_result(:, :)*100/(4000);
end
clear answ cns;
end
end

plot impedance results
h_imp_zones=figure;
subplot(1,3,1)
plot(Zab(:,1), 'Marker','o', 'Color','blu'); hold on;
% plot(filtered_Zab(:,1), 'Marker','o', 'Color','magenta'); hold
on;

subplot(1,3,2)
plot(Zbc(:,1), 'Marker','o', 'Color','red'); hold on;
subplot(1,3,3)
plot(Zca(:,1), 'Marker','o', 'Color','yellow'); hold on;

for i=1:No_Nodes
    subplot(1,3,1)

plot(real(zd_bus(i,1)), imag(zd_bus(i,1)), 'Marker','diamond', 'Color','magenta');
hold on;

text(real(zd_bus(i,1)), imag(zd_bus(i,1)), string(i));
subplot(1,3,2)

plot(real(zd_bus(i,1)), imag(zd_bus(i,1)), 'Marker','diamond', 'Color','magenta');
hold on;

text(real(zd_bus(i,1)), imag(zd_bus(i,1)), string(i));
subplot(1,3,3)

plot(real(zd_bus(i,1)), imag(zd_bus(i,1)), 'Marker','diamond', 'Color','magenta');
hold on;

text(real(zd_bus(i,1)), imag(zd_bus(i,1)), string(i));

end

%
for i=1:No_Nodes
    subplot(1,3,1)
    if MHO_ab_result(i,1)>0

plot(polygon_ab(i,1:2:10), polygon_ab(i,2:2:10), 'Color','green', LineWidth=1);

```

```

        hold on;
    end
    subplot(1,3,2)
    if MHO_bc_result(i,1)>0

plot(polygon_bc(i,1:2:10),polygon_bc(i,2:2:10),'Color','green',LineWidth=1);
        hold on;
    end
    subplot(1,3,3)
    if MHO_ca_result(i,1)>0

plot(polygon_ca(i,1:2:10),polygon_ca(i,2:2:10),'Color','green',LineWidth=1);
        hold on;
    end
end

subplot(1,3,1)
ylim([-0.05,(max(polygon_ab(:,2:2:10),[],'all')*1.2)])
xlim([-0.05,(max(polygon_ab(:,1:2:10),[],'all')*1.2)])
legend('Zab','Zd behind of the busses');
title('Zab loop impedance [ohm]');
xlabel('R [ohm]');
ylabel('X [ohm]');
subplot(1,3,2)
ylim([-0.05,(max(polygon_bc(:,2:2:10),[],'all')*1.2)])
xlim([-0.05,(max(polygon_bc(:,1:2:10),[],'all')*1.2)])
legend('Zbc','Zd behind of the busses');
title('Zbc loop impedance [ohm]');
xlabel('R [ohm]');
ylabel('X [ohm]');
subplot(1,3,3)
ylim([-0.05,(max(polygon_ca(:,2:2:10),[],'all')*1.2)])
xlim([-0.05,(max(polygon_ca(:,1:2:10),[],'all')*1.2)])
legend('Zca','Zd behind of the busses');
title('Zca loop impedance [ohm]');
xlabel('R [ohm]');
ylabel('X [ohm]');

end

```

8.1.3 DFT FUNCTION

```

%% Function DFT_v7
% the news is that v5 don't need the input of N_samples and pre_fault
% (hyp that pre_fault doesn't change the
%%
% it takes the line-to-line voltages (Oscillo) and the residual voltage at
% the secondary of the TV (0-100 [V]) and it calculates the star voltages
% in time, the phasors of them and then move to the (d,i,0) seq. components
% thanks to Fortescue transform. It returns the (d,i,0) voltages seq.
% evolution recorded by the oscillo

```

```
%Vn input in [V]
function [Ea, Eb, Ec, E0,Ed,Ei,Ia, Ib, Ic, I0,Id,Ii] = DFT_v7 (Vn,waveform)

%% finding the N_samples
index_zerocrossing1=0;index_zerocrossing2=0; j=1;
for i=1:height(waveform)-1

    if waveform(i,2)<= 0 && waveform(i+1,2)>= 0

        index_zerocrossing2=i;

    end

    if index_zerocrossing1 ~= index_zerocrossing2
        N_samples1(j) = index_zerocrossing2-index_zerocrossing1;
        j=j+1;
    end
    index_zerocrossing1 = index_zerocrossing2;
end
N_samples = 400;
%%
%Fortescue matrix
alfa = exp(1i*(2/3)*pi); %angle shift for fortescue matrix
F = (1/3)*[1 1 1; 1 alfa alfa^2; 1 alfa^2 alfa]; %inverse fortescue matrix

Et(:,1)=waveform(:,4)*1000;
Es(:,1)=waveform(:,3)*1000;
Er(:,1)=waveform(:,2)*1000;
L = length(Er(:,1));

Ea=zeros(L,1);
Eb=zeros(L,1);
Ec=zeros(L,1);

% Initializing fortescue transformation-> (d,i,0) sequences
I0 = zeros(L-N_samples,3);
Id = zeros(L-N_samples,3);
Ii = zeros(L-N_samples,3);

%% fft() of the star voltages and fortescue transformation-> (d,i,0)
sequences
E0 = zeros(L-N_samples,3);
Ed = zeros(L-N_samples,3);
Ei = zeros(L-N_samples,3);

%% DFT code

for i=1:L-N_samples

    k=1;
```

```

for n=0:N_samples-1
    Ea(i,1)=Ea(i,1)+Er(n,i,1)*exp(-1i*k*2*pi*(1/N_samples)*(n));
    Eb(i,1)=Eb(i,1)+Es(n,i,1)*exp(-1i*k*2*pi*(1/N_samples)*(n));
    Ec(i,1)=Ec(i,1)+Et(n,i,1)*exp(-1i*k*2*pi*(1/N_samples)*(n));
end
Ea(i,1)=Ea(i,1)*(2/(N_samples*sqrt(2)));
Eb(i,1)=Eb(i,1)*(2/(N_samples*sqrt(2)));
Ec(i,1)=Ec(i,1)*(2/(N_samples*sqrt(2)));

%(0,d,i) calc using inverse fortescue matrix F
A = F*[Ea(i,1); Eb(i,1); Ec(i,1)];
%multiply by 1000 to get parameters in [V], from [kV]
E0(i,1) = A(1);
Ed(i,1) = A(2);
Ei(i,1) = A(3);

end

% Calculation of magnitude and angle of the (d,i,o) seq. components
E0(:,2) = abs(E0(:,1));
E0(:,3) = angle(E0(:,1));
Ed(:,2) = abs(Ed(:,1));
Ed(:,3) = angle(Ed(:,1));
Ei(:,2) = abs(Ei(:,1));
Ei(:,3) = angle(Ei(:,1));

%% CURRENTS
%initializing the arrays to store the currents
Ia=zeros(L,1);
Ib=zeros(L,1);
Ic=zeros(L,1);

% Initializing fortescue transformation-> (d,i,0) sequences
I0 = zeros(L-N_samples,3);
Id = zeros(L-N_samples,3);
Ii = zeros(L-N_samples,3);
%Importing values
Ir=waveform(:,5)*1000;
Is=waveform(:,6)*1000;
It=waveform(:,7)*1000;

%DFT code
for i=1:L-N_samples

    k=1;
    for n=0:N_samples-1
        Ia(i,1)=Ia(i,1)+Ir(n,i,1)*exp(-1i*k*2*pi*(1/N_samples)*(n));
        Ib(i,1)=Ib(i,1)+Is(n,i,1)*exp(-1i*k*2*pi*(1/N_samples)*(n));
        Ic(i,1)=Ic(i,1)+It(n,i,1)*exp(-1i*k*2*pi*(1/N_samples)*(n));
    end
    Ia(i,1)=Ia(i,1)*(2/(N_samples*sqrt(2)));
    Ib(i,1)=Ib(i,1)*(2/(N_samples*sqrt(2)));

```

```

Ic(i,1)=Ic(i,1)*(2/(N_samples*sqrt(2)));

%(0,d,i) calc using inverse fortescue matrix F
A = F*[Ia(i,1); Ib(i,1); Ic(i,1)];
%multiply by 1000 to get parameters in [A], from [kA]
I0(i,1) = A(1);
Id(i,1) = A(2);
Ii(i,1) = A(3);

% Calculation of magnitude and angle of the (d,i,o) seq. components
I0(:,2) = abs(I0(:,1));
I0(:,3) = angle(I0(:,1));
Id(:,2) = abs(Id(:,1));
Id(:,3) = angle(Id(:,1));
Ii(:,2) = abs(Ii(:,1));
Ii(:,3) = angle(Ii(:,1));

end

figure
subplot(2,1,1)
plot(waveform(:,5))
hold on;
plot(waveform(:,6))
hold on;
plot(waveform(:,7))
hold on;
% plot(waveform(:,8))
hold off;
title('Currents in time')
legend('Ir(t)', 'Is(t)', 'It(t)')
Y=1.1*sqrt(2)*Vn/1000;
ylim([-Y Y])

subplot(2,1,2)
plot(I0(:,2))
hold on;
plot(Id(:,2))
hold on;
plot(Ii(:,2))
hold off;
title('magnitude RMS of (d,i,o) sequence components Currents')
legend('I0_{rms}', 'Id_{rms}', 'Ii_{rms}')

%% plot of line-to-ground voltages

h_waveforms=figure;
subplot(3,1,1)
plot(waveform(:,2))
hold on;
plot(waveform(:,3))
hold on;

```

```

plot(waveform(:,4))
hold on;
% plot(V0_prim(:,1))
hold off;
title('star voltages in time')
legend('Vr(t)', 'Vs(t)', 'Vt(t)')
Y=1.1*sqrt(2)*Vn;
% ylim([-Y Y])

subplot(3,1,2)
plot(1:1:length(Ea(:,1)),abs(Ea(:,1)))
hold on;
plot(1:1:length(Eb(:,1)),abs(Eb(:,1)))
hold on;
plot(1:1:length(Ec(:,1)),abs(Ec(:,1)))
hold off;
title('star voltages in time')
legend('Er(rms)', 'Es(rms)', 'Et(rms)')
% ylim([-Y Y])
%
%
subplot(3,1,3)
plot(E0(:,2))
hold on;
plot(Ed(:,2))
hold on;
plot(Ei(:,2))
hold off;
% ylim([0 Y/sqrt(3)])
title('magnitude RMS of (d,i,o) sequence components (star voltages)')
legend('E0_{rms}', 'Ed_{rms}', 'Ei_{rms}')

end

```

8.1.4 FAULT CLASSIFIER

```

%% Fault classifier

function Fc =
fault_classifier(Vn_ll,Ed,Ei,Eo,TetaEd,TetaEi,TetaEo,Id,Ii,Io,TetaId,TetaIi,TetaIo)
% It receives as input (d,i,o) seq components (magnitudes and phase
% displacement and it calculates which fault it is

En = Vn_ll/sqrt(3); %rated line-to-ground voltages
k=9/10; %to calculate the thresholds
o_seq = 0;
i_seq = 0;

%Check the zero sequence voltage presence
if (Eo>(En*(1-k)))

```

```

        o_seq=1;
    end
    %Check the inverse sequence voltage presence
    if (Ei>(En*(1-k)))
        i_seq=1;
    end

    Fc='Error';

    %in case of null o-seq. we have an unground fault (LLL, LL)
    if (o_seq==0 && i_seq==0 && Ed<=(k*En))
        Fc='LLL';
    elseif (o_seq==0 && i_seq==0 && Ed>(k*En))
        Fc='No_fault';
    elseif (o_seq==0 && i_seq==1)
        Fc='LL';
    end

    %in case of not-null o-seq. we have a ground fault (LG, LLG)
    if(o_seq==1)
        Sum1 = Ed*cos(TetaEd)+ Eo*cos(TetaEo)+ Ei*cos(TetaEi);
        Sum2 = Ed* sin(TetaEd)+ Eo*sin(TetaEo)+ Ei*sin(TetaEi);
        if i_seq==0 % SLG faults should not have inverse sequence!
            if (abs(Sum1) < Vn_ll*0.01) && (abs(Sum2) < 0.01*Vn_ll)
                Fc='LG';
            end
        elseif i_seq==1
            Fc='LLG';
        end
    end
end
end

```